THREE-ELECTRODE ELECTROCHEMICAL APPROACH FOR DEGRADATION ANALYSIS FOR LITHIUM-ION BATTERIES

A Thesis

by

ROBERT DANIEL MINTER

Submitted to the Office of Graduate and Professional Studies of
Texas A&M University
in partial fulfillment of the requirements for the degree of

MASTER OF SCIENCE

Chair of Committee,	Partha P. Mukherjee
Committee Members,	Sarbajit Banerjee
	Hong Liang
Head of Department,	Andreas A. Polycarpou

August 2017

Major Subject: Mechanical Engineering

ABSTRACT

Lithium-ion batteries are becoming increasingly important as increases in power and energy density pave the wave for them to replace more traditional energy storage systems. Understanding the degradation phenomena that occurs in lithium-ion batteries is important because it allows for the continual improvement in both safety and performance of these complicated systems. A three-electrode system is a powerful method to characterize the degradation phenomena since it allows the study of the decoupled effects of the cathode and anode electrodes.

The objective of this research is to diagnosis and prevent degradation phenomena occurring in lithium-ion batteries. This is done through a multiple step process which includes the development of a reliable three-electrode experimental setup, the electrochemical characterization of the cell through use of potential and electrochemical impedance spectroscopy measurements, and the application of this knowledge to prevent lithium plating and improve cell performance by implementing anode potential based control.

From the anode potential measurements, it was found that the anode potential reached negative values during high C-rate charging. This could then be used to identify the existence of lithium plating. This identification then formed the foundation for the anode-based control. From the impedance measurements, the individual electrode contributions to the overall cell impedance were characterized and were used to explain the changes in cell impedance as a function of the cell state of charge.

After successfully characterizing the lithium-ion cell through potential and impedance data, anode potential based control was implemented which utilized both the anode potential and full cell voltage readings to prevent lithium plating and prevent cell overcharging, simultaneously. The cell capacity retention was improved by limiting the anode potential above a certain threshold value. This showed that lithium plating was occurring and the capacity retention of the cell could be improved by prevention of these degradation phenomena.

ACKNOWLEDGEMENTS

I would like to thank my committee chair, Dr. Partha P. Mukherjee for his support and guidance throughout my studies with him as a M.S. student. Without him and his ambition for groundbreaking research, this work would not be possible. I would also like to thank my committee members, Dr. Hong Liang and Dr. Sarbajit Banerjee, for their support and guidance throughout my research.

I would also like to thank my colleagues at the Energy and Transport and Sciences Lab at Texas A&M University for their continuous discussions, help, and guidance. Specifically, I would like to thank Daniel Juarez-Robles, Chien-Fan Chen, Sobana Rangarajan, Aashutosh Mistry, and Michael Kalan. In addition, many others not named here were of great help and I would like to thank you all as well.

Finally, thanks to my family for their support in my decision to continue my education into graduate school. Without their support, I would never have succeeded.

CONTRIBUTORS AND FUNDING SOURCES

Contributors

Part 1, faculty committee recognition

This work was supervised by a thesis committee consisting of Professor Partha P. Mukherjee [advisor], Professor Hong Liang [committee member] of the Department of Mechanical Engineering, and Professor Sarbajit Banerjee [committee member] of the Department of Chemistry.

Part 2, student/collaborator contributions

All work for the thesis was completed independently by the student.

Funding Sources

Financial support from Texas Instruments (TI) University Research Partnership program is gratefully acknowledged.

NOMENCLATURE

EC	Electrochemical Capacitor
EDL	Electrical Double Layer
SEI	Solid Electrolyte Interphase
LTO	Lithium Titanate, $Li_4Ti_5O_{12}$
RE	Reference Electrode
PVDF	Polyvinylidene Fluoride
NMP	N-methyl-2-pyrrolidinone
EIS	Electrochemical Impedance Spectroscopy
SOC	State of Charge
CC	Constant-Current
CV	Constant-Voltage
CCCV	Constant-Current and Constant-Voltage
FRA	Frequency Response Analyzer
LTM	Laplace Transform Method

TABLE OF CONTENTS

Page

LIST OF FIGURES

Page

CHAPTER I

INTRODUCTION AND LITERATURE REVIEW

INTRODUCTION TO ENERGY STORAGE

Energy storage is an important aspect of technology and is vital to the continued operation of our society as a whole. In recent years, there has been a large push towards using renewable energy sources such as wind or solar power in lieu of non-renewable sources, such as oil and natural gas. One of the main problems with using renewable sources of energy is that they are not consistently or reliably available. One very valuable aspect of energy storage devices is the ability to store the energy generated from renewable energy sources, when it is available, and allow it to be used at a later unspecified time. In this way, energy storage devices can be integrated into existing systems to supplement traditional energy generation methods. Some of the main problems for energy storage systems are installation costs, durability and reliability, and round-trip efficiencies [1-15]. Moving forward, one possibility is that the energy generated from renewable energy sources can be collected, stored, and eventually entirely replace nonrenewable sources.

The sources from which we obtain and consume energy varies and each method has its own respective benefits and drawbacks. Some of the sources include solar, nuclear, hydro, wind, geothermal, natural gas, coal, biomass, and petroleum. Each of these sources are used for different energy sectors. One of the problems with traditional energy production is the amount of waste energy generated. Combustion of petroleum products produces a

lot of waste heat as well as pollution into the environment. A schematic of the various energy production methods in the United States in 2016 is shown in Figure 1.

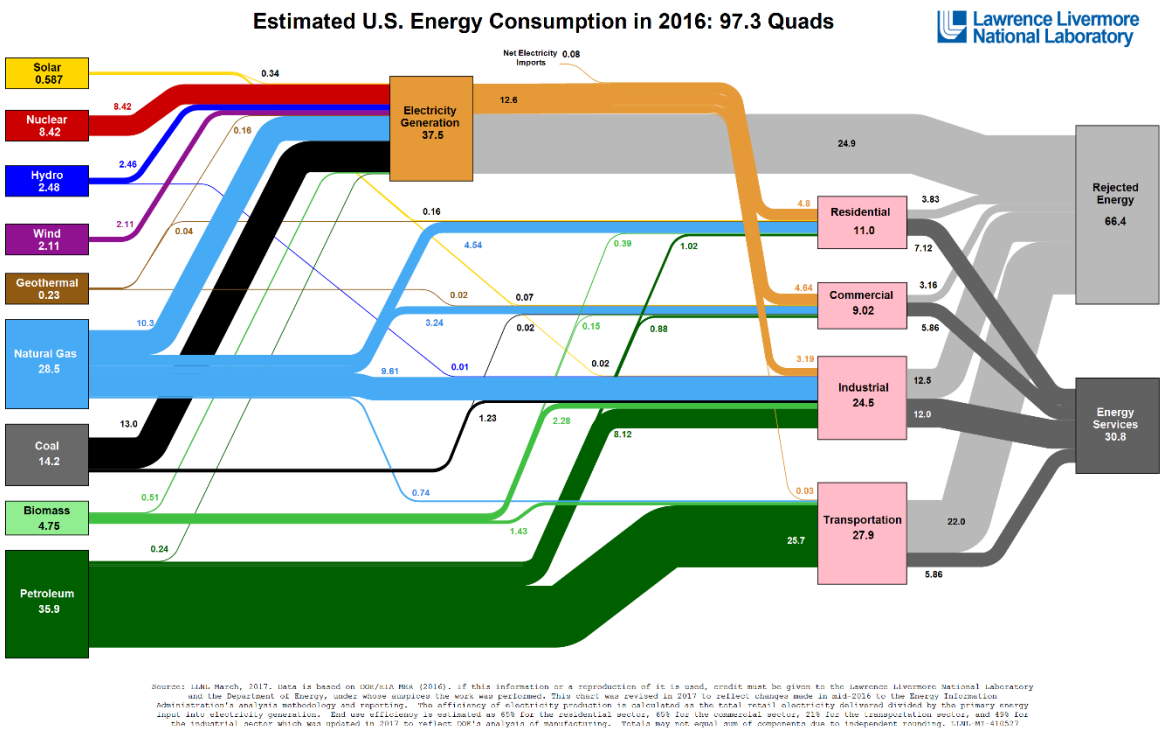

Figure 1. Estimated energy consumption in the United States in 2016. Reprinted from Lawrence Livermore National Laboratory

ENERGY STORAGE SYSTEMS

Energy storage systems can take many different forms: from the very simple to the very complex. A few examples include chemical, electrochemical, and mechanical energy storage. A simple mechanical energy storage system could be a compressed spring. A

certain amount of energy must be input into the system to compress the spring, and then the spring is locked into place. The amount of energy stored in this system can be approximated using Hooke's Law. In order to release the energy in this system, the spring must be unlocked and allowed to expand. The force of this spring expanding can provide useful work for another application. In this case, the compressed spring provides a very simple example of an energy storage device.

ELECTROCHEMICAL ENERGY STORAGE

Electrochemical energy storage devices are another major area of energy storage. Devices in this category usually belong to one of three groups: batteries, electrochemical capacitors (also known as ultracapacitors or supercapacitors), and fuel cells. All three of these devices operate in a very similar fashion. All three have a positive electrode, a negative electrode, and an electrolyte. Both batteries and fuel cells operate by converting chemical energy into electrical energy via a redox reaction that occurs at each of the two electrodes. A battery is a closed system, meaning no mass transfers across the system boundaries, where a fuel cell is an open system, meaning mass is transferred across the system boundaries. A fuel cell has a continuous transfer of fuel through the system to provide the energy while a battery contains all of the stored energy inside of the electrodes themselves. An electrochemical capacitor (EC) is slightly different in that the energy is stored in an electrical double layer (EDL) which exists at the surface between the electrode and electrolyte. The EDL is essentially a separation of positive and negative charge that occurs at the electrode-electrolyte interface. The energy storage in the form of an electric field is

the same principle of operation of an electrical capacitor, hence the similar naming scheme. The generation and release of this separation of charge in an EC is what provides the energy storage mechanism [16-22].

COMPARISON OF ENERGY STORAGE SYSTEMS

Each of the three electrochemical energy storage groups has benefits and drawbacks. Some of these tradeoffs can be succinctly summarized by using a Ragone plot. A Ragone plot comparing the performance of batteries, fuel cells, ECs, traditional capacitors, and their relation to internal combustion engines is shown in Figure 2.

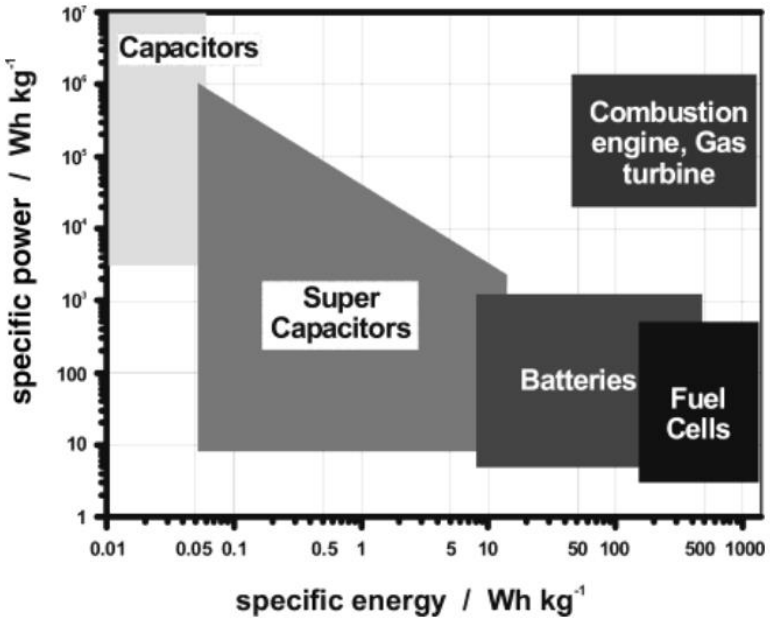

Figure 2. Ragone Plot comparing performance of common electrochemical energy storage devices in terms of power and energy provided. Reprinted from Chemical Reviews, vol. 105 [16]

From the Ragone plot we can see two important parameters: how much energy each device can store (specific energy), and how quickly the energy can be provided (specific power). These characteristics have value for different systems, including portable systems, where specific energy is important, and high-demand applications, where specific power is important. In some situations, one example being use in electric vehicles, both energy and power are of utmost important. The Ragone plot is one way to compare the relative benefits and drawbacks of the three electrochemical storage devices concerning energy and power. ECs have a very high specific power because the energy is stored in the EDL and not with a faradaic reaction, which has additional limiting factors regarding the conversion of energy, for example the reaction kinetics or the solid state diffusion inside of the electrode [16]. The drawback of an EC is that not as much energy can be stored using the EDL and thus they have a lower overall energy storage capability. Fuel cells have a much higher energy storage capacity but much lower power. The continuous consumption of fuel leads to high energy but fuel cells require auxiliary power systems, pumps, and storage vessels which limit the overall power available per unit mass (or volume). Batteries hold the middle ground, providing intermediate energy and power capacities. From Figure 2 it is obvious that all three of these devices fall short of providing both the energy and power provided by a traditional combustion engine or gas turbine. The focus of many areas of research has become trying to improve upon the performance of electrochemical energy devices in order to provide the power and energy demanded by many applications and eventually replace other more traditional systems.

More specifically, batteries have gained a lot of interest in current research due to their potential to replace other systems and their use in more demanding applications such as electric and hybrid-electric vehicles. Important factors to consider with battery systems are power density, energy density, safety, and cycle life [4, 23-26]. In a very general sense, a battery is a device that converts chemical energy into electrical energy. Electrical energy is arguably the most useful energy source for our everyday lives because it can be readily used to power our technological devices. Batteries can be useful to aid in the storage and collection of renewable energy sources as well as providing grid-scale power backups. Batteries are also very useful in providing power to our portable devices, such as cell phones, laptops, and automobiles. With recent technological improvements, such as the increasing development of advanced lithium-ion batteries, the energy and power provided by these systems is large enough to replace some of the more traditional systems in use.

In order to understand how a battery works, it is important to understand its constituents. A battery has several main components that all work together during its operation. The most important components of a battery are the electrodes and the electrolyte. There are other components of the cell that depend on the form factor, such as gaskets, separators, internal springs, additional protection circuits, and other miscellaneous components, but these do not contribute electrochemically to the operation of the cell. They serve other purposes such as providing a sealed environment, increasing the internal pressure inside the cell, or serving as safety or protective measures.

Batteries can come in many different form factors, or sizes. Some of the most common form factors are prismatic, coin cells, and cylindrical cells. Figure 3 shows some examples of batteries found in everyday applications. Although very different in shape and size, the different battery form factors include all of the basic components and are governed by the same fundamental operation.

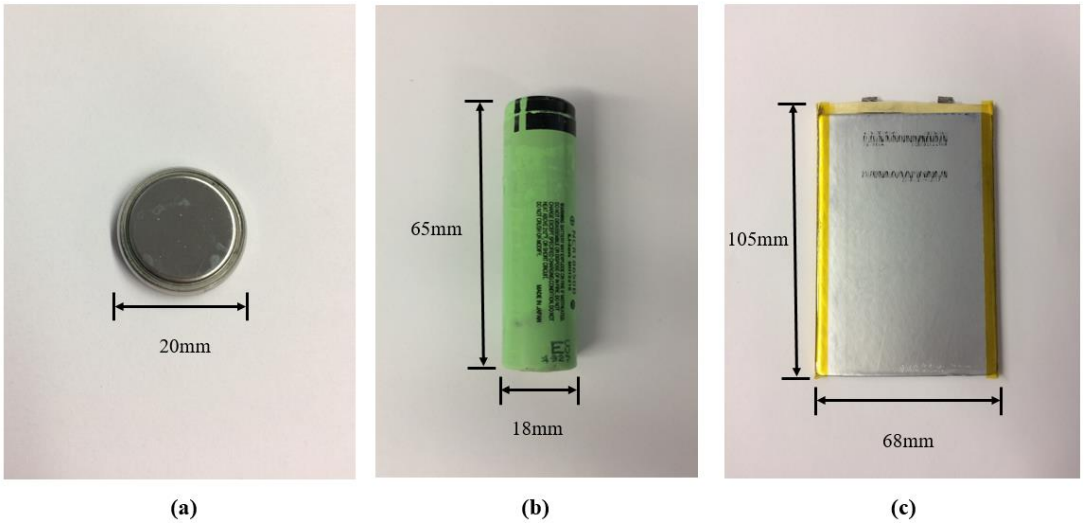

Figure 3. Various form factors for batteries including (a) coin cell, (b) cylindrical, and (c) prismatic/pouch

As was mentioned earlier, a battery converts chemical energy into electrical energy. The driving force for this conversion of chemical energy into electrical energy is the electrochemical potential difference between the cathode and anode, which is dictated by

thermodynamics. The difference in potential is the driving force for an electrochemical reaction at the electrode-electrolyte interface. The difference between an electrochemical reaction and a chemical reaction is that the electrochemical reaction takes place at two different locations and is a surface driven phenomenon. At one electrode, an oxidation reaction takes place and at the other electrode, a reduction reaction takes place. Whether the oxidation or reduction reaction occurs at the cathode or anode depends on whether the cell is being charged or discharged, i.e. whether the cell is operating as an electrolytic or galvanic cell. A chemical reaction, by contrast, takes place in the bulk and is a volumetric driven phenomenon.

During discharging, a reduction reaction occurs at the anode and an electron and ion are produced. The electron flows through an external circuit and provides useful work in the form of electrical energy. The ion stays inside of the battery and migrates from the anode, through the separator/electrolyte, and into the cathode. At the cathode, an oxidation reaction occurs, and the ion reunites with an electron. The movement of ions inside the battery and the movement of electrons in the external circuit must balance, that is, there is a conservation of charge due to the entire system remaining electronically neutral.

LITHIUM-ION BATTERIES

The lithium-ion battery is the subject of this thesis; therefore, a short summary of the specifics of its operation is appropriate. For the lithium-ion battery system, lithium ions are the charge carriers of the system. A schematic of a lithium-ion battery system is shown in Figure 4. The lithium-ion system is an intercalation chemistry, meaning that the charge

carriers, lithium ions, are stored inside the host structures of the electrode materials as lithium. During discharge, the lithium and electron disassociate and move from the anode to cathode; during charge the lithium ion and electron move from the cathode to the anode. The flow of electrons in the external circuit is harvested as electrical energy (when discharging) and used to power the selected application.

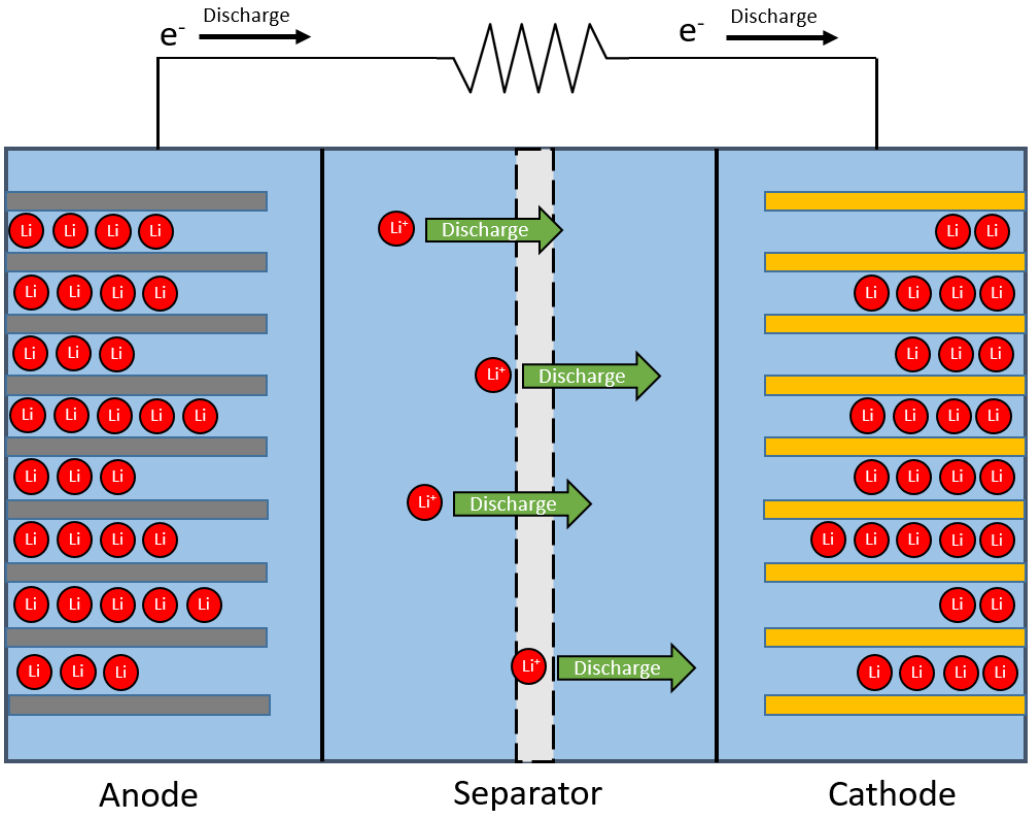

Figure 4. Schematic of a lithium-ion battery during discharging process

The intercalation characteristics of the lithium-ion battery are important because they govern many of the limitations of the system [27-30]. The intercalation and subsequent mass diffusion of lithium inside the solid electrode structure is often a limiting factor in the operation of the cell. Higher electrode porosity may lead to higher mass diffusion inside the electrode, but will generally result in a lower volumetric energy storage capacity. Much like in many fundamental areas in science, everything is a tradeoff.

DEGRADATION PHENOMENA IN LITHIUM-ION BATTERIES

Other major issues associated with lithium-ion batteries are the major degradation phenomena. Some examples include formation of the solid electrolyte interphase (SEI) layer, volumetric expansion and mechanical damage (mentioned earlier), lithium plating and dendrite formation, electrolyte decomposition, and other side reactions that can occur either in the electrolyte or at the electrodes [31-47]. Other issues include dissolution or corrosion of the current collectors, electronic isolation of active materials, and binder decomposition [48, 49]. A schematic detailing some of the various types of degradation phenomena can be seen in Figure 5.

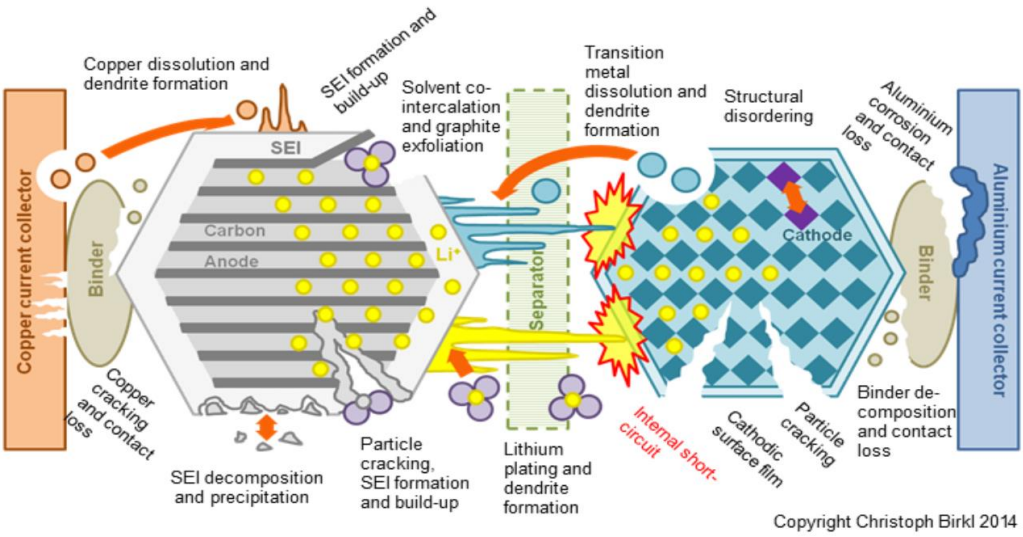

Figure 5. Various types of degradation phenomena occurring for lithium-ion batteries. Reprinted from Journal of Power Sources, vol. 341 [43]

The solid electrolyte interphase (SEI) is a thin film that typically forms on anodes in lithium-ion batteries. It is the result of the decomposition of the electrolyte and occurs at the anode specifically due to the electrochemical potential of the anode existing below the lower electrochemical potential stability window of the electrolyte. The film itself increases in the ohmic resistance of the cell and thus has some negative effects on the cell performance. The formation of the SEI also involves the consumption of some of the active lithium in the system and thus often shows up as an initial capacity fade during the initial cycling of a cell [50-54]. The benefit of the SEI is that it improves the stability of the overall system and prevents further reaction of the electrolyte, which would have a

negative effect on cell performance [49, 55-57]. Research by Buqa et al. has shown that the performance of the graphite anodes and the formation of their SEI can be improved by virtue of a surface pre-treatment, and suggested it might be related to the roughened morphology of the graphite surface [51]. In general, the SEI allows the passage of lithium ions in the system and thus is a necessary component for lithium-ion batteries. A schematic showing the SEI layer forming on a graphite electrode is shown in Figure 6. This figure shows that the solvent in the electrolyte reacts with the lithium in the anode, and results in a thin SEI film between the electrolyte and electrode surface.

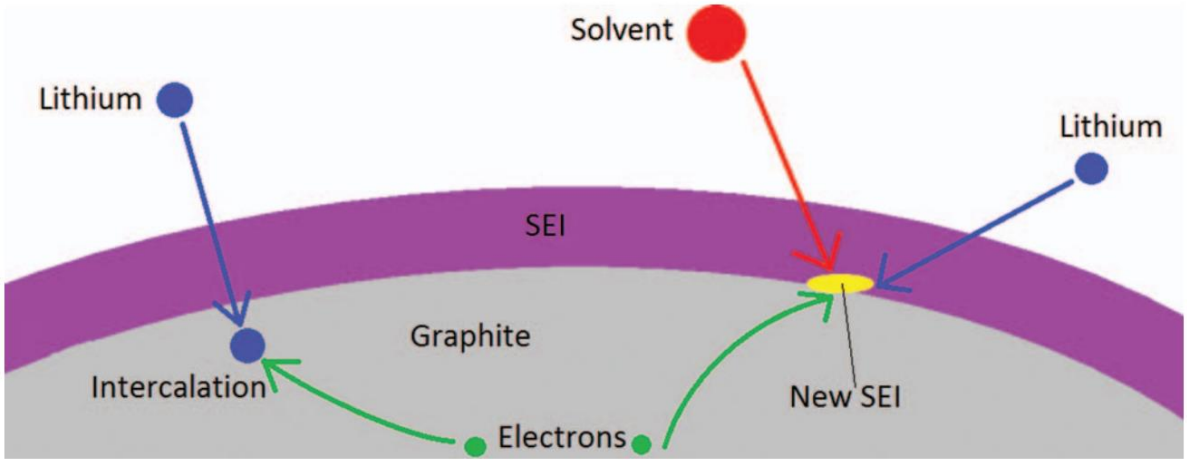

Figure 6. Schematic showing the reaction occurring between the electrolyte and anode, resulting in a solid electrolyte interphase (SEI) layer. Reprinted from Journal of the Electrochemical Society, vol. 160 [58]

Another degradation phenomenon that is related to the intercalation of lithium into an electrode material is the internal stresses that are generated due to the occupation of the void spaces in the atomic structure [59]. Note that once inside the structure, the lithium ion and electron converge and produce Li, and not Li^+. Therefore, lithium ions are the charge carrier in the cell but they are stored as regular lithium in the electrodes. The volumetric expansion is not as big a problem for carbon-based electrodes due to the relatively small magnitude of the expansion but can become a big problem for other chemistries such as copper-tin ($LiCu_6Sn_5$) [60-67] or lithium-sulfur (LiS) [11, 68-70]. In fact, this volumetric expansion and the subsequent mechanical stresses represent a major challenge to the use of these chemistries in practical systems. Because the battery is a closed system, the system is constrained when it expands, which results in internally generated stresses. These stresses can then lead to cracking and mechanical damage of the electrode material. The issues with volumetric expansion and the subsequent mechanical damage often show up as poor cycling performance, as isolation of active material or mechanical damage to the structure reduces available electrochemical capacity in the system. The mechanical cracking and damage to the electrode structure has been modeled by some research groups; one example of this modeling is shown in Figure 7. The figure shows the difference between the crack formation for a graphite particle, which has relatively small volumetric expansion and subsequent crack formation, and a silicon particle which has considerably higher volumetric expansion and commensurate crack formation.

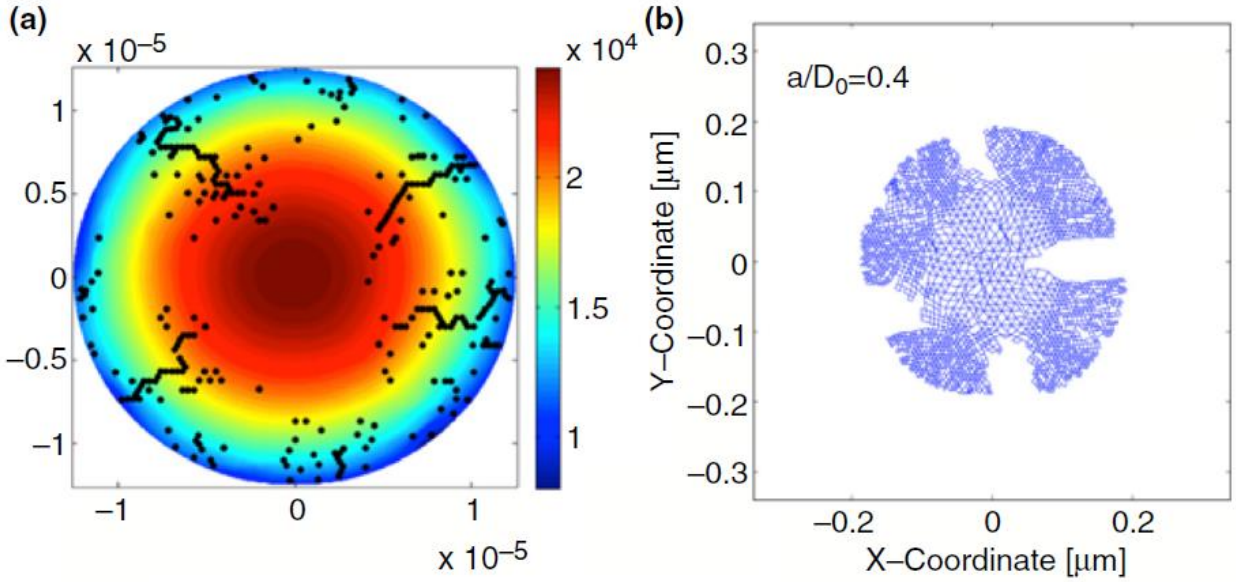

Figure 7. Crack formation modeling shown for (a) graphite and (b) silicon electrode particles. Reprinted from Current Opinion in Chemical Engineering, vol. 13 [52]

Another common degradation phenomenon that plagues lithium-ion batteries is lithium plating and dendrite formation. Lithium plating is when instead of intercalating into the host electrode structure, lithium deposits on the surface of the structure as either a (relatively) uniform metallic layer (plating) or small dendritic structures. Plating can have effects ranging from causing safety issues to impeding cycling performance [39, 71-83].

From a phenomenological perspective, lithium plating occurs due to an inability of the lithium to intercalate into the host electrode structure effectively. Plating tends to occur at low temperature, high charging rate, high electrode state of charge (SOC), or a combination of these three factors [84]. At low temperature, the solid state diffusion inside

of the electrode is reduced, due to the Arrhenius diffusivity dependence on temperature. The lower solid state diffusion results in a buildup of lithium at the electrode-electrolyte interface and a subsequent deposition of lithium. At a high charging rate, a similar phenomenon occurs. The lithium is attempting to intercalate into the electrode structure very quickly, but is unable to and thus is plated. At a higher SOC, there is on average less space for the lithium to intercalate into the structure, and thus it becomes more favorable to deposit on the surface.

Lithium dendrites are of particular importance due to the safety concern they cause. If dendrites form inside of a cell, there is a potential for them to grow, pierce the separator, and cause an internal short between the anode and cathode. This internal short leads to a very high localized temperature which then leads to thermal runaway, which can result in an explosion of the cell. Other issues related to dendrite formation is the increased surface area of the reactive lithium. The lithium will react with the electrolyte and cause increased SEI formation, which will lead to increased capacity loss. A schematic of lithium dendrite formation is shown in Figure 8.

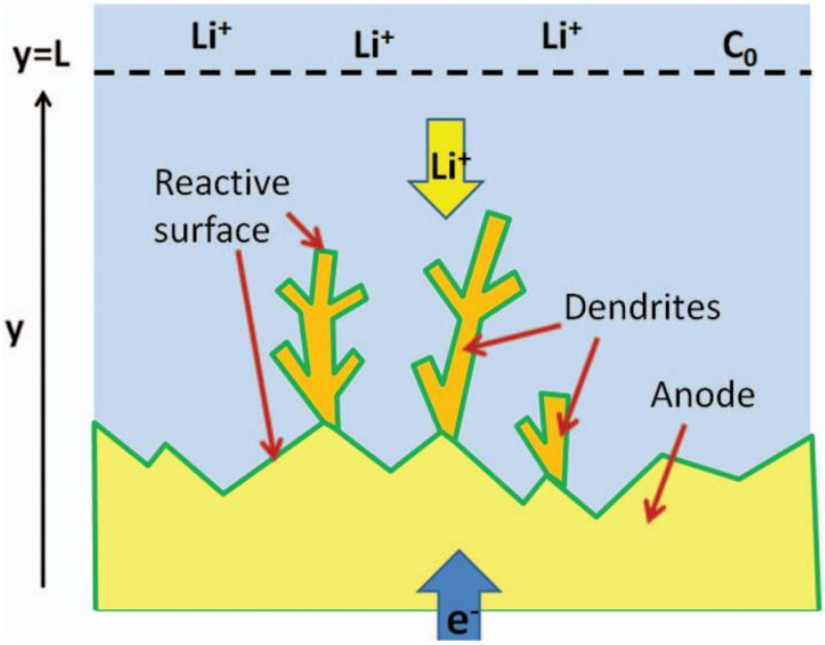

Figure 8. Dendrites forming on the surface between the anode and electrolyte. Reprinted from Journal of the Electrochemical Society, vol. 163 [85]

Studying the various degradation effects that occur in lithium-ion batteries can be a difficult task. One of the main problems is that the operation of the entire cell is a complex, coupled process that involves the simultaneous behavior and response of the cathode and anode. For example, it is impossible to study degradation in the anode without taking into account the effects of the other electrode. In addition, in a typical battery, only the full cell voltage of the cell can be measured, and not the individual electrode potentials. A method that provides greater detail and insight into the cell operation is therefore needed for a more fundamental study of the degradation effects inside of a lithium-ion battery.

INTRODUCTION TO THREE-ELECTRODE CELLS

A three-electrode setup is a very powerful method to decouple the two electrode's response and provide a greater insight into the fundamental physics of the battery operation. In a three-electrode setup, a reference electrode is introduced in addition to the cathode and anode. This reference electrode is then used to measure the potential of the anode and cathode dynamically during operation. No current is passed through the reference electrode and hence, it provides a singular, and ideally stable, voltage. By using a three-electrode setup, the full cell voltage, the cathode potential, and the anode potential can be collected simultaneously during operation.

The purpose of this thesis is to use a three-electrode setup to characterize and study the degradation occurring in lithium-ion batteries. The first step towards achieving this goal, then, is to perform a literature review to better understand the current and past research towards accomplishing this objective. This literature review will be discussed next.

The objective of this section is to provide a comprehensive literature review that covers the research done by other groups involving three-electrode cells and their respective methods of characterizing degradation in lithium-ion batteries.

One of the first steps in creating a three-electrode coin cell setup is to select the reference electrode. Lithium metal is a very common reference electrode because it is relatively easy to procure and use, and allows the reading of electrode potentials vs Li/Li^+ directly. It is very convenient to use because the entire chemistry of the lithium-ion battery system is

based on the electrochemical potential of lithium metal. One of the downsides of using lithium metal as a reference directly is its high polarizability, which can lead to inaccurate measurements [86]. Other groups have claimed success in using lithium metal reference electrodes in aging studies [87], but recommend against leaving the reference inserted during the actual aging process. This hints towards one of the problems with using lithium metal: its instability. Part of the problem is the growth of the SEI layer on the lithium electrode is unavoidable. Other issues involve the fact that the lithium, along with its unavoidable passivating layer, have a large impedance that can cause errors associated with impedance measurements of individual electrodes.

Some groups have attempted to improve upon the shortcomings of lithium metal electrodes by modifying the electrode material itself. Solchenbach et al. has alloyed lithium and gold to produce a reference electrode which they claim is suitable for long-term impedance and potential measurements [88]. Research by Jansen et al. been focused towards low-temperature characterization by using a lithium-tin reference electrode [89]. Other research by Abraham et al. was aimed at determining impedance contributions of electrodes and also used a lithium-tin alloy reference electrode [90]. Some research has been aimed at studying lithium titanate ($Li_4Ti_5O_{12}$), which can function as both an anode and reference electrode due to the very stable plateau it exhibits throughout a wide state of charge [91-95].

In addition to the material itself, there are other logistical issues associated with the size and placement of the reference electrode inside of the cell. In general, a smaller reference

electrode is desirable as it minimizes the influence on the overall cell, which should operate in an identical fashion to a regular two-electrode cell. There may be some interference due to the inclusion of the reference electrode, but this should be minimized. Research by Dees et al. has shown that the size and location of the reference electrode inside of the cell has a significant impact on the impedance measurements [96]. Constructing three-electrode coin cells can be difficult as the coin cell form factor has been shown to display a wide variety of uncertainty, depending on the alignment and size of the electrodes [97].

Many research groups have worked on creating their own custom three-electrode cells [84, 98-102] but they often include difficult and expensive setups. There is a great need to design a simple, effective, and reliable three-electrode setup that can accomplish all of the desired needs.

CHAPTER II

EXPERIMENTAL SETUP

OVERVIEW

The objective of this chapter is to describe the methodology used in the creation and optimization of the experimental three-electrode setup. This three-electrode setup is the basis for all of the data collected, and thus it forms the backbone for this work.

The process can be divided into several main steps: the preparation of the reference electrode, the lithiation of the reference electrode in a preparation cell, and the construction of the final three-electrode cell. The development of the process was iterative, in that improvements were continually made as the setup was being developed. Along the process of development, there were many failures, and these were used to improve the reliability and success rate of the construction process. An overall schematic of the process can be seen below in Figure 9.

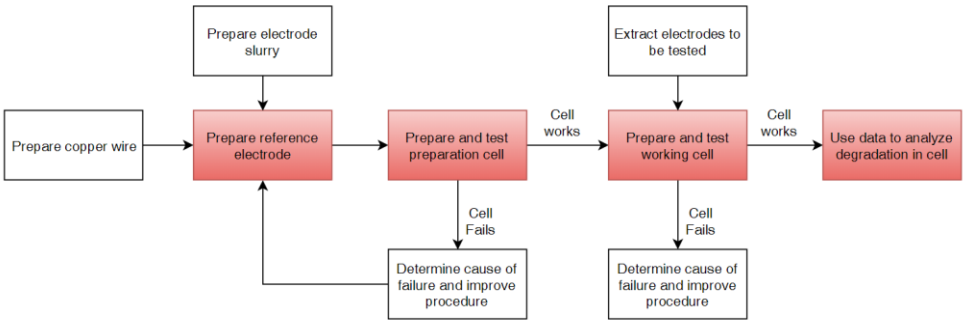

Figure 9. Overview of the three-electrode construction process

The steps shown in red are the major steps in the process. The first three are covered in this chapter of the thesis and the final data analysis is covered in the following two chapters.

REFERENCE ELECTRODE PREPARATION

Before beginning the preparation of the reference electrode, a material was selected. As discussed in the first chapter, many research groups choose to use lithium metal, despite the many drawbacks it has. For this work, lithium titanate ($Li_4Ti_5O_{12}$), herein abbreviated as LTO, was chosen as the active material. This is because it displays a potential plateau (measured around 1.56 V) for a very wide state of charge [92, 93]. Thus, if the reference is charged to the middle of this potential plateau, it has greater resistance to accidental perturbations to the state of charge.

Using the active material, a slurry was prepared which also included a conductive additive (carbon powder) to increase the electrical conductivity, and a binder (polyvinylidene fluoride, PVDF) which binds all of the particles together. The solvent that was used to mix all of the powders and binder together was N-methyl-2-pyrrolidone (NMP).

In addition to the active material, there must also be a current collector. An insulated copper wire was chosen due to the high electrical conductivity of copper (i.e. a minimal resistance). The insulation is important because without it the wire could short with other components inside of the final cell.

After the preparation of the current collector, the slurry was cast onto the tip of the wire. The wire and slurry then combine to form the reference electrode used in the actual cells. The reference electrode was dried in an oven at 70°C for a minimum of 4 hours. After drying, the reference can be used. Instructions for the preparation of the reference electrode, including more details, follows.

1. Wire Preparation
    a. Cut one 12-centimeter length of size 32 AWG (0.202 mm diameter) enameled copper wire. Each wire will become one reference electrode and will be used inside of one three-electrode cell.
    b. Place one end of the wire in a laboratory press. Gently press approximately 1 cm of wire at one end to a pressure of about 4 MPa.
    c. Cut the excess wire off of the wire tip so that the flattened section is about 2 mm in length. The average thickness of the tip is approximately 0.1 mm. Be careful not to bend the flattened tip as it may fatigue and break off.
    d. Place the wire on a Teflon cutting board and carefully use a scalpel to remove the outer insulation on the flattened wire tip. Make sure to remove the insulation from both sides. The final product should be a flat, shiny section of exposed copper.
    e. Weigh the wire using a laboratory scale. This mass will be used after the slurry has been cast to determine exact amount of electrode material present in each reference electrode.

f. Repeat steps a-e for a typical batch size of 36 wires.

g. Place the wires on a receptacle for storage. A good option is to tape the wires around the edge of a small glass jar, where each jar can comfortably hold 12 wires. An example of this method of storage is shown in Figure 10.

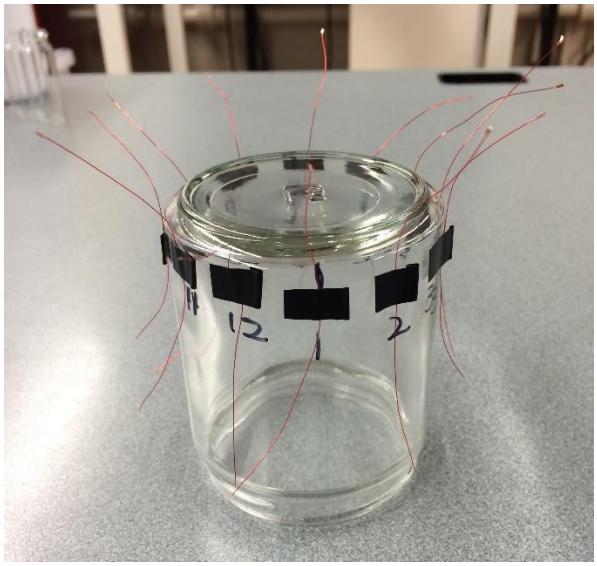

Figure 10. Storage of reference electrode wires around a small glass jar. The top end of the wire will be coated with the electrode slurry and become the completed reference electrode.

2. Slurry Preparation

   a. First, prepare the 10% wt. polyvinylidene fluoride (PVDF) solution in N-methyl-2-pyrrolidinone (NMP).

b. Clean a stainless steel scoop with isopropyl alcohol prior to use. This is done to ensure there is no contamination of the source material from an unclean scoop.
c. Using a small rectangular weigh paper, the stainless steel scoop, and a laboratory scale, measure out the desired mass of PVDF powder (0.1 g).
d. Transfer the PVDF powder from the weigh paper into a 500 ml plastic bottle.
e. Measure and transfer the appropriate mass of NMP liquid (0.9 g) into the bottle by using a 1 ml capacity laboratory pipette.
f. Insert a magnetic stirring bar into the solution; place the bottle on a magnetic stirring plate, and leave to mix indefinitely. Allow the solution to mix for at least 24 hours prior to the first use. It is recommended to prepare the PVDF solution in bulk to avoid having to make smaller batches for each slurry batch.
g. Before weighing any more powder, clean the stainless steel scoop, the pestle, and the mortar with isopropyl alcohol to avoid any contamination.
h. Using a weigh paper, the laboratory scale, and the stainless steel scoop, measure out the appropriate amount (0.8 g) of lithium titanate ($Li_4Ti_5O_{12}$) powder. Carefully transfer the powder to the mortar and pestle. Clean the scoop with isopropyl alcohol after use.

i. Using the same method as step h), weigh out the appropriate amount (0.03 g) of KS-6 synthetic graphite. Carefully transfer the powder to the same mortar and pestle and clean the scoop with isopropyl alcohol as before.

j. Lightly mix the three powders in the mortar until they become uniformly dispersed. They should appear as in Figure 11.

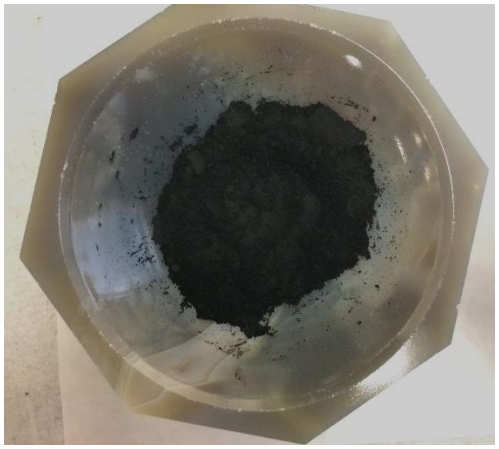

Figure 11. Uniformly mixed powders consisting of active material, conductive additive, and graphite additive

k. Grind the powder mix using the pestle until the mixture becomes homogenous.

l. Carefully transfer the powder mix to a 20 ml disposable mixing tube. This will serve as a high-shear mixing vessel to ensure homogeneous distribution of all the materials inside the slurry.

m. Add the appropriate amount of NMP (2.2 ml) to the mixing tube using a laboratory pipette. Add sixteen 6 mm diameter silicate glass mixing balls and screw on the cap.

n. Place the mixing tube on the high-shear mixing device, lock the tube into place, and mix the slurry for 15 minutes on the maximum setting (about 6000 rpm).

o. Add 0.8 g of the PVDF solution (prepared earlier) to the mixing tube. Continue mixing the slurry for another 5 minutes to ensure even distribution of binder.

p. Immediately cast the slurry on the wires. If the slurry sits for longer than 5 minutes, mix the slurry for an additional 15 minutes prior to use to ensure a homogeneous mixture.

3. Casting and Drying of Reference Electrode

    a. Carefully dip the exposed copper at the tip of each reference electrode into the mixed slurry. Another option is to drop-cast the slurry from a pipette onto the wire tip. Be careful to only coat the flattened, exposed section of the copper wire.

    b. Place the reference electrodes into a laboratory oven at 70°C. Allow at least 8 hours for the electrodes to completely dry. After drying, transfer the reference electrodes into the inert argon glovebox for use in the cell manufacturing process.

The progression of the reference electrode wire tip, from the original wire to the final product can be seen in Figure 12.

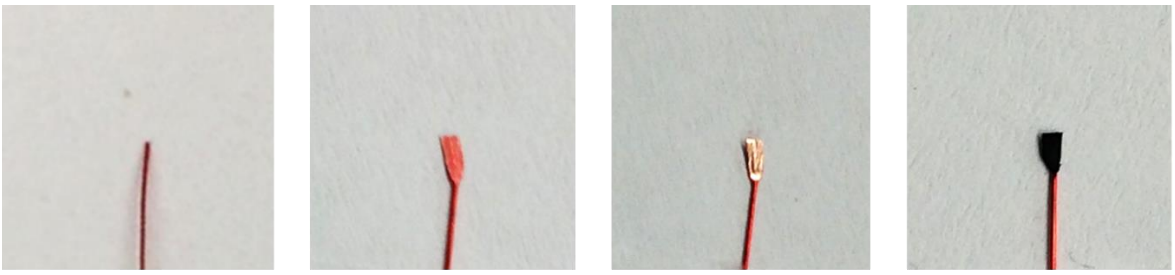

Figure 12. Progression of the reference electrode showing (a) original wire, (b) pressed wire, (c) wire with insulation removed, and (d) wire with electrode cast and dried; complete electrode

CONSTRUCTION OF THE PREPARATION CELL

After the reference electrodes are properly prepared. The next step is to construct the preparation cell. The preparation cell is used to determine the stability of the reference electrode as well as to determine the plateau voltage. This plateau voltage is then used to recalibrate the potential measurements when the final three-electrode cell, also known as the working cell, is constructed. After the reference electrode is lithiated (i.e. charged and discharged) inside of the preparation cell, the preparation cell is opened inside of the glovebox and the reference electrode is harvested and used for the final setup. The preparation cell is thus sacrificial, but necessary in order to accurately determine the

plateau voltage. The following is a description of the process used to construct and lithiate the preparation cell.

1. First, prepare the reference electrode by using a pair of pliers to bend the wire into a spiral shape. Make sure that the final spiral shape will fit inside of the gasket of the coin cell (approximately 1.56 cm diameter). The extra wire spiral provides stability and will also be unfolded and later used in the working cell. An image of the final wire shape is shown in Figure 13.

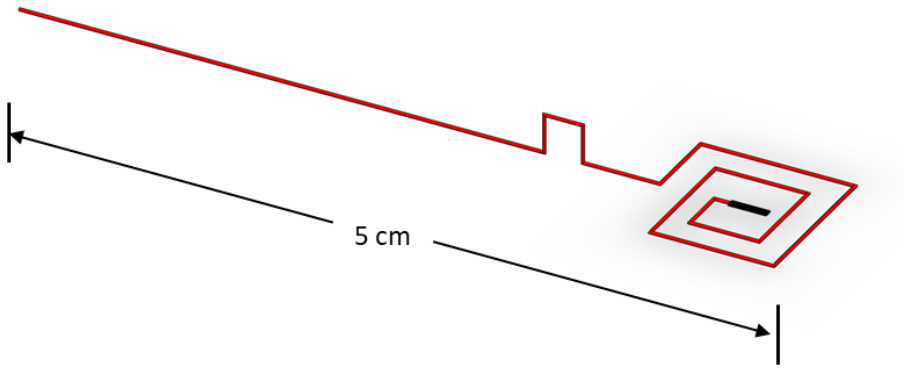

Figure 13. Spiral shaped reference electrode used in the preparation cell. The small rectangular notch in the wire is for where it exits the coin cell.

2. Place each electrode spiral into a small weigh boat and set aside.
3. Clean both sides of a lithium metal ribbon by using a scalpel or a razor blade. Scrape off any surface oxidation until the shiny lithium shows through. Make sure

to clean both sides of the lithium. Take extreme caution when using sharp objects inside of the glovebox.

4. Punch out two 1.56 cm discs for each cell from the cleaned lithium ribbon using the hollow punch.
5. Center one disc of lithium on a 0.5 mm stainless steel spacer. Press the lithium metal and the spacer firmly together.
6. Place the coin cell case inside of a small weigh boat. Fit the second disc of lithium inside of the coin cell case. Make sure the lithium is centered and press firmly so that the lithium sticks to the case.
7. Place several drops electrolyte (1.0 M LiPF6 in EC/DEC (1:1 by vol.)) on the lithium disc and several drops around the edge of the lithium to fill the outside gap. If not enough electrolyte is added there will be bubbles under the separator and inside of the cell, which is undesirable.
8. Place one 1.905 cm PP separator on top of the wetted lithium disc. Make sure that separator is completely wetted and there are no bubbles trapped underneath.
9. Place the gasket in the cell with the gasket lip facing upwards. This lip is where the cap will seat into. Press firmly to fit the gasket into the case.
10. Using a pair of plastic tweezers, gently place the reference electrode spiral into the center of the cell. Add a few drops of electrolyte around the reference electrode.
11. Place a small square rectangle of separator on top of where the wire crosses over the gasket and the cell case. This helps prevent shorting between the wire and the metal cell cap.

12. Place one 1.59 cm separator on top of the reference electrode spiral. Make sure the separator is completely wetted and that there are no bubbles trapped underneath.
13. Place the lithium-spacer disc on top of the reference electrode, lithium side facing downwards.
14. Place the wave spring on top of the spacer. Make sure all components are centered inside of the cell.
15. Fill the cell to the brim with electrolyte. When the cell is crimped, the extra electrolyte will be squeezed out.
16. Using plastic tweezers carefully place the cell cap on top of the assembly. Press firmly to seat the cap into the lip of the gasket.
17. Bend the reference electrode wire such that it lays flat over the top of the cap. This is done to make sure the wire is not cut short when crimping the cell.
18. Carefully transfer the cell to the coin cell crimping device by using a plastic tweezers. When transporting, hold the cell flat to avoid the loss of any additional electrolyte.
19. Crimp the coin cell to approximately 5 MPa.
20. Remove the coin cell from the crimper and bend the exposed wire back up away from the top of the cell. This is to avoid any possible shorting between the cap and the reference electrode.
21. Remove the completed coin cell from the Argon glovebox. Using isopropyl alcohol and a lint-free task wiper, carefully clean the cell exterior. Take care to avoid disturbing the wire and the location where the wire exits the cell.

22. Cell Sealing

a. Carefully dry the coin cell using a lint-free task wiper. Take extra care to dry the location where the wire exits the coin cell.
b. Mix equal parts resin and hardener to form a non-conductive epoxy.
c. Using a toothpick or small probing device, carefully apply a small amount of epoxy to the location where the wire exits the coin cell. This is the location where the cell is most likely to leak.
d. Allow one hour for the epoxy to dry before connecting to any testing equipment. Note that it can take upwards of 24 hours for the epoxy to fully cure and harden. However, the purpose of the epoxy here is to seal the cell and not to provide any mechanical strength.

23. Lithiation Procedure

a. Connection Setup
    i. Using a handheld lighter, burn about 2 cm of insulation off at the end of the reference electrode wire protruding from the cell. This is where the wire will connect to the testing device. Bend the exposed wire back on itself; this helps improve the connection when connecting the three-electrode cell for testing.
    ii. Place a small square of electrical tape (2 cm × 2 cm) across the top of the coin cell case. This should prevent electrical contact between the top of the coin cell and the coin cell holder.

iii. Place the preparation cell in the cell holder. The top of the cell should be insulated from any connection and the bottom of the cell should be connected to the negative reading on the cell holder.

iv. Using an alligator clip, connect the reference electrode to the top clip on the cell holder (positive connection). The cell should be set up to test with the reference electrode acting as the positive electrode and the bottom lithium disc (cell case) acting as the negative electrode.

b. Reference calibration voltage

i. Calculate the amount of active material present for the reference electrode. For a typical electrode mass of 1 mg and an 80% active material composition, this comes out to 0.8 mg.

ii. Using the active material mass and the theoretical specific capacity of lithium titanate [103], determine the appropriate current to charge the cell at C/16.

iii. Cycle the reference electrode several times between the appropriate voltage range (1.25-2.25 V) at C/16. This value will change depending on the specific reference electrode in use.

iv. Take note of the plateau voltage / reference voltage, which should occur during both the charging and discharging processes. For a $Li_4Ti_5O_{12}$ electrode this value is typically around 1.56 V versus Li/Li_+.

v. Record the reference voltage and the corresponding cell with which it is associated. This voltage will be used to calibrate the potential of the electrodes when used in a working cell.

24. Rest the cell for 24 hours and monitor that the reference electrode potential is steady.

An example of a completed lithiation voltage profile is shown in Figure 14.

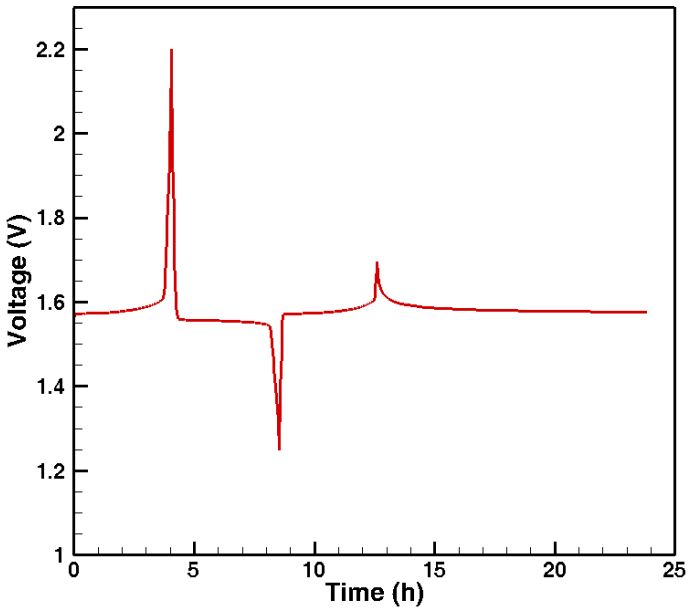

Figure 14. Complete lithiation for the preparation cell. Note the existence of the plateau voltage around 1.56 V, which becomes stable after the cell has been resting for many hours.

25. Transfer the lithiated cell into the inert argon environment for use in the working cell construction. Avoid any possible contact between the reference electrode and the cap or the cell case. This could short the reference electrode and alter its potential.

The completed coin cell can be seen in Figure 15.

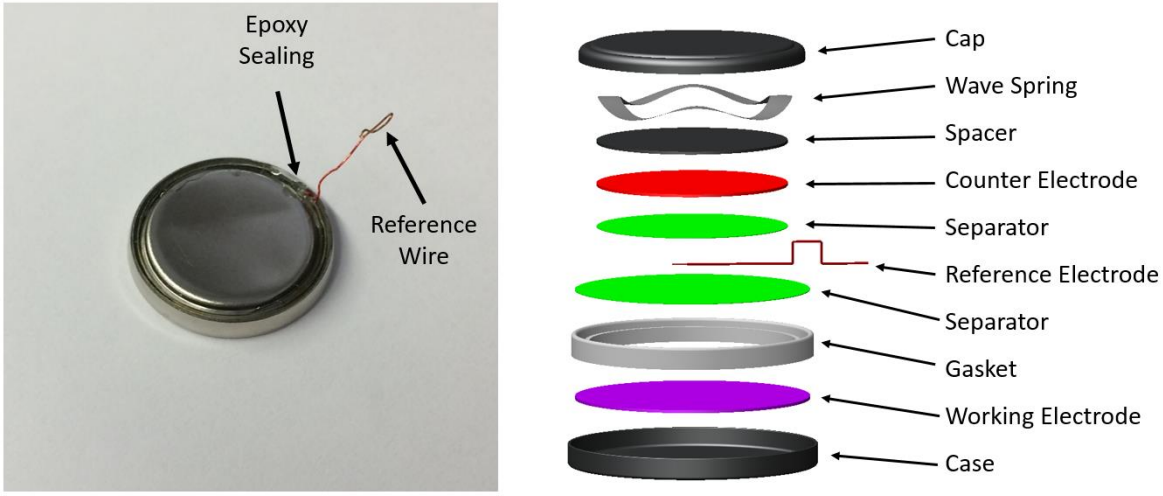

Figure 15. Completed three-electrode coin cell setup showing internal layout of the components.

The location where the wire exits the cell is vital because the wire is pressed between the case, the cap, and the gasket. The wire must not short with the case or the cap, otherwise

the cathode or anode will be shorted with the reference. A close-up view of how exactly the wire exits the cell can be seen in Figure 16.

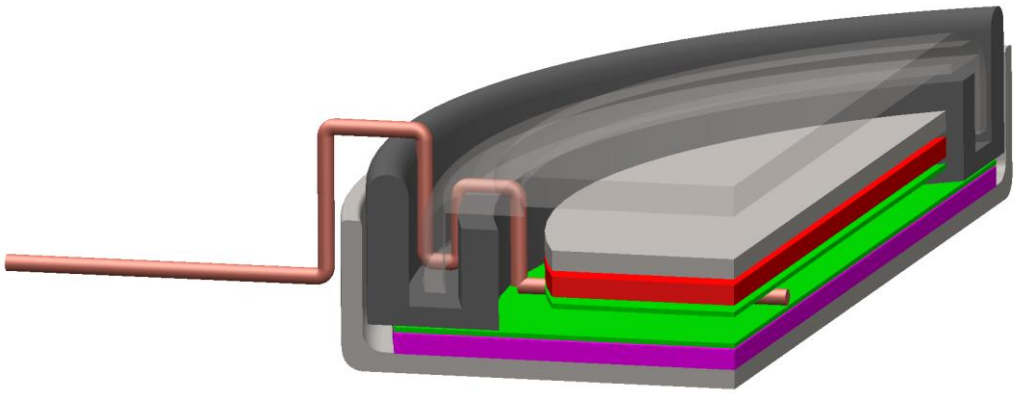

Figure 16. Three-electrode coin cell showing the entry point of the reference electrode as well as the internal layout. Note that in this figure, the cap is transparent and the wave spring (not shown) is located just above the top spacer.

CONSTRUCTION OF THE WORKING CELL

After the preparation cell has been constructed and properly lithiated, the reference contained within will be used for the final working cell. The plateau voltage collected during the lithiation process is used for the calibration of the cathode and anode potential readings. The working cell is the end goal of the experimental procedure. The objective of the working cell is to collect information regarding the electrodes (the cathode and/or

anode) by using the reference electrode. The procedure describing the construction of the working cell is as follows.

1. Place the coin cell case inside of a small weigh boat. Place the cathode disk in the center of the cell case. Place several drops of the DEC electrolyte on the cathode and several drops around the edge to fil the outside gap.
2. Place one 19.05 mm separator on top of the electrode. Make sure the separator is completely wetted and that there are no bubbles trapped underneath.
3. Place the gasket with the small lip for the cell cap facing upwards. Press firmly to properly fit the gasket into the case. Set the coin cell assembly aside and locate the lithiated preparation cell.
4. Extract the lithiated reference electrode.
    a. Apply a small square of electrical tape to the top of the lithiated preparation cell. This helps prevent shorting between the case and cap during disassembly.
    b. Hold the preparation cell firmly, with the cap side facing up, by using the thin-nosed pliers. Be careful not to short the cell with the metal pliers.
    c. Use the end-cutting pliers to carefully, yet firmly, pry open the coin cell along the edge. Take care not to short the top and bottom of the cell with the metal pliers. Hold the cell as demonstrated in Figure 17.

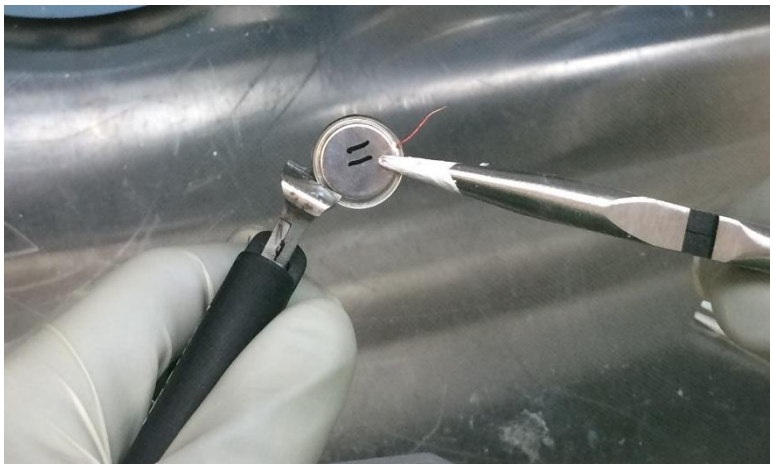

Figure 17. Opening of the preparation cell and extraction of the reference electrode

d. Once approximately 70% of the cell has been pried open, hold the case with the end-cutting pliers and carefully separate the cell case and cap using the thin-nosed pliers.
e. Carefully extract the lithiated reference electrode and discard the other cell components.

5. Using a pair of pliers, bend the reference electrode and wire such that it sits in the center of the electrode. Cut off the exposed, uninsulated wire.
6. Add a few drops of electrolyte on and around the reference electrode.
7. Place a small rectangular separator on top of where the wire crosses over the gasket and cell case. This helps prevent shorting between the wire and the metal case and cap.

8. Place another small square of separator on top of the tip of the reference electrode. This helps to prevent shorting between the reference electrode and the anode.
9. Place the prepared anode disc on top of the reference electrode in the cell. Take care to properly align the shape of the cathode with that of the anode. The reference electrode tip should be in the center and the wire should exit in the rectangular gap.
10. Carefully place the 1.0 mm stainless steel separator on top of the anode.
11. Place the wave spring on top of the spacer. Make sure all the components are centered in the cell.
12. Fill the cell to the brim with electrolyte.
13. Using plastic tweezers, carefully place the cell cap on top of the assembly. Press firmly down to seat the cap into the lip of the gasket.
14. Carefully fold the remaining wire back over the cell cap prior to crimping. This prevents the wire from being cut off during crimping.
15. Carefully transfer the cell to the coin cell crimping device by using a pair of plastic tweezers. When transferring the cell, make sure to keep it flat to avoid the loss of additional electrolyte.
16. Crimp the cell to approximately 5 MPa.
17. Remove the coin cell from the Argon glovebox. Carefully clean the cell using isopropyl alcohol and a lint-free task wiper.
18. Cell Sealing
    a. Carefully dry the coin cell using a lint-free task wiper. Take extra care to dry the location where the wire exits the coin cell.

b. Mix equal parts resin and hardener to form a non-conductive epoxy.
c. Using a toothpick, carefully apply a small amount of epoxy to the location where the wire exits the coin cell. This is the location where the cell is most likely to leak.
d. Allow one hour for the epoxy to dry before connecting to any testing equipment. Note that it can take upwards of 24 hours for the epoxy to fully cure and harden. However, the purpose of the epoxy here is to seal the cell and not to provide any mechanical strength.

CONNECTION FOR ELECTROCHEMICAL TESTING

Although the major presentation of results and analysis is discussed in the next two chapters, the basic connection methodology is discussed here. This is an important step in order to collect accurate and repeatable results as well as avoid damaging the cell. If the connection is setup incorrectly, for example if the reference electrode is connected as either a working or counter electrode, the cell could be destroyed.

The following discusses the connection for the various tests conducted in this work: namely voltage/potential measurements and impedance characterization. Each test is important because it allows different aspects of the cell to be studied. For example, the potential measurement of the anode can be used to detect lithium plating, while the anode impedance can characterize the effect of the plating on the impedance contribution of the anode, especially in comparison to the cathode and full cell. The steps to connect the cell for these tests is as follows.

1. Performance and Cycling
    a. Calculate the theoretical capacity for the both the cathode and anode electrodes.
    b. Using the total dry weight of the electrode disc, the mass of the aluminum/copper substrate, and the weight percentage of active material, determine the mass of active material present for each electrode.
    c. Determine the capacity of each electrode by multiplying the mass of active material by its respective theoretical capacity. Using the most limiting electrode capacity (typically the cathode), determine the overall cell capacity.
    d. Connect the cell to the electrochemical measuring device, taking care with connecting: positive power and positive sense to cathode, negative power and sense to anode. The reference should be connected to the reference electrode via the copper wire. A schematic of the connection can be seen in Figure 18.

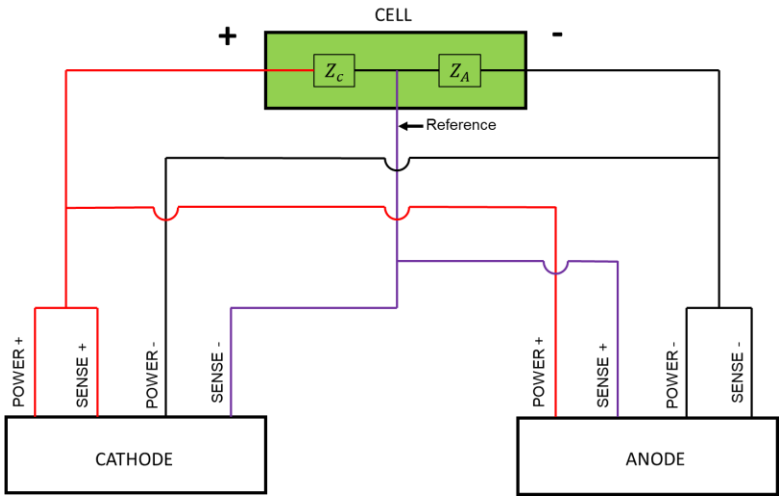

Figure 18. Voltage and potential measurement connection for the three-electrode cell. Note that the full cell positive power and sense connect to the cathode, and the full cell negative power and sense connect to the cathode.

e. Double check that the cell is connected and working properly by checking the open circuit voltage and potentials. Use the reference voltage recorded during the lithiation procedure to calibrate the cathode and anode potential readings.

f. Cycle the full cell at the desired C-rate, for example C/10, and measure the full cell, cathode, and anode potentials simultaneously.

g. Repeat steps a-f for other cells and C-rates as desired, depending on the specifications and requirements for each cell.

2. Electrochemical Impedance Spectroscopy

   a. Full Cell Impedance

i. Connect the cell to the EIS measurement device with the following: positive power and positive sense to cathode, negative power and sense to anode. The reference should be connected to the reference electrode via the copper wire. Note: a general schematic of the impedance connection can be seen in Figure 19.

ii. Select potentiostatic control for the EIS with a frequency amplitude of 10 mV.

iii. Select a frequency range of 1MHz to 1mHz. Note that this range may not always be required and can be modified after collecting preliminary results.

iv. Collect impedance of the full cell. Plot a Nyquist plot and Bode plot to analyze the response of the cell.

b. Cathode Impedance

i. Connect the cell to the EIS measurement device with the following: positive power and positive sense to cathode, negative power and negative sense to anode, and reference to reference electrode.

ii. Repeat the same steps as for the full cell impedance (aii-aiv).

c. Anode Impedance

i. Connect the cell to the EIS measurement device with the following: positive power and positive sense to anode, negative power and negative sense to anode, and reference to reference electrode.

ii. Repeat the same steps as for the full cell impedance (aii-aiv)

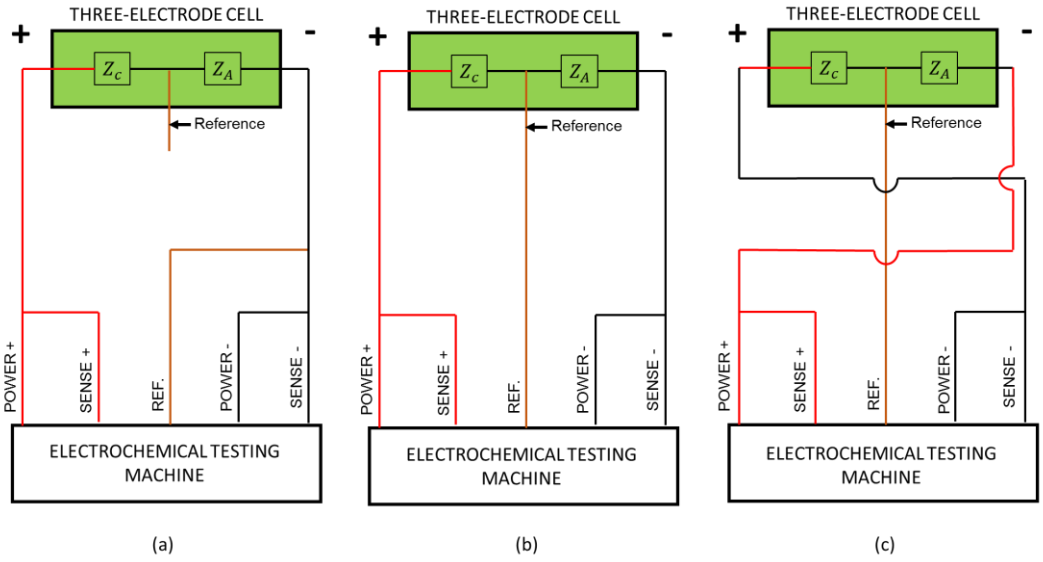

Figure 19. Connection to the electrochemical testing machine to measure impedance for (a) full cell, Z_F, (b) cathode, Z_C, and (c) anode, Z_A.

3. Impedance as a function of State of Charge
    a. Connect the cell to the EIS measurement device according to the desired impedance measurement: either full cell, cathode, or anode
    b. Charge the cell using constant current at C/2 until the cell reaches the upper voltage limit. Hold the voltage at the upper limit using a constant voltage control method until the applied current drops below C/100. The cell should now be fully charged.
    c. Discharge the cell at C/2 for 3 minutes; the cell should now be at 90% state of charge (SOC). Allow the cell to rest for 1 hour to reach equilibrium conditions.

d. Collect the impedance using the same procedure described previously, depending on whether the full cell, cathode, or anode impedance is described.
e. Repeat steps c-d to collect the impedance as a function of the state of charge.

DISCUSSION

The following is a discussion regarding the experimental setup process as a whole. There are many subtle adjustments which were made in order to increase the success rate of the cells. During preliminary development of the process, the success rate was as low as 25%. After fine tuning and optimizing the processing variables, the success rate became as high as 80%. Thus, it is important to discuss the important variables and tips that can be used to ensure a reliable, and successful cell construction.

Cell crimping pressure plays an important part in the success rate of both the preparation and working cells. If the cell is crimped at too high of a pressure (>800 psi) the reference electrode can become shorted with the cell cap due to the reference wire position in-between the cap and gasket. Note that the wire crossing this interface is a requirement in order to connect the reference electrode reading to an external measurement device. If the cell pressure is too low (<700 psi) the cell can have issues with incomplete crimping which may cause electrolyte leakage and air penetration after the cell is removed from the inert argon environment. It was found that around 750 psi is the optimal pressure for crimping the cell to avoid leaking or shorting issues. In order to provide additional means to prevent

these issues with shorting of the reference wire, a vital step in the construction process is the additional square separator that is placed along the gasket where the wire crosses the cell boundary. This separator provides an additional insulating layer that helps prevent internal shorting. In addition, slightly different crimping pressures may be required for the preparation and working cell. The preparation cell uses two lithium discs that are significantly thicker than an electrode cast on a metal foil – which are used in the preparation cell.

After the lithiation of the reference electrode in the preparation cell, the reference electrode must be extracted and reused in the working cell. During this process, extreme care must be taken. In general, if the reference electrode was prepared properly, there should not be any issue associated with adhesion of the material to the flattened section of the wire. In any case, the amount of time between when the reference electrode is removed from the preparation cell and used in the working cell should be minimized. The reference electrode should not be placed on any surface or allowed to rest outside for a significant amount of time. Minimizing manipulation of the wire is ideal because it avoids possible fatiguing and breaking of the wire.

Another important consideration when constructing the three-electrode coin cell is sealing the cell properly. Because the wire is sandwiched between the cap and gasket, there is potential for a small breach in the cell that may allow for electrolyte leakage or air penetration in the cell. If this is not rectified, distortion may be seen in the impedance measurements and the entire cell may fail due to reactions with the environment,

especially after an extended period outside of the inert glovebox in which it is fabricated. In the cell construction procedure, the use of the non-conductive epoxy is vital because it completely seals the cell from the outside environment. One interesting observation is that if the cell is not crimped to a high enough pressure, the epoxy will not harden properly and will sometimes bubble up. This may be caused by the electrolyte being wicked up and mixing with the epoxy, or the higher internal pressure of the cell slowly leaking out and causing bubbles form. Note that the epoxy, both during and after hardening, was soaked in the electrolyte and no obvious sign of any reaction was observed. If used properly, the epoxy-sealed cell should be allowed to dry for a minimum of 1 hour inside of the glovebox before removal. Afterwards the epoxy can harden in an atmospheric environment. Depending on the epoxy used, it may take 24 hours or more for the epoxy to fully cure, and during this process, the cell should be allowed to rest. In the event that the cell is not sealed or the sealing procedure is not sufficient, the cell will leak into the environment. After a while, the cell may begin to change colors. An example of poorly sealed cells can be seen in Figure 20.

Figure 20 Improperly sealed three-electrode coin cells, demonstrating leaking and resultant reaction of the electrolyte with the environment.

When constructing the three-electrode coin cells, the shape of the host electrodes can play an influence on the performance of the cell. Various possible shapes can be seen in Figure 4. In an ideal case, the reference electrode would be placed at the center of the electrodes. Some problems that can occur involve an uneven pressure distribution within the cell due to location of the reference electrode. Another issue is that the existence of the reference electrode between the host electrodes creates an artificial increase in the cell impedance, due to the fact that the reference is blocking a portion of the electrode area. Some configurations, (Figure 4 c-f) attempt to reduce this issue by carving out a small area in

which the reference can sit. The problem is that this reduces the cell capacity as well as introduces complexity in the manufacturing process.

When connecting the three-electrode cell to the electrochemical testing measurement, the connection to the reference electrode can be very sensitive due to the small diameter of the copper wire used. Note that the wire diameter must be small in order to reduce any effects on the cell performance, one of which could be a blockage of the area between the two planar electrode disks. Because of this connection sensitivity, it is advantageous to bend the exposed end of the copper wire back on itself multiple times to increase the surface area for connection. If this is not done, the reference electrode may appear to be shorted or have failed, when in fact the cell is working as expected.

One limitation of using a three-electrode coin cell is that the entire process is done by hand. A certain amount of practice is required when constructing coin cells in order to produce consistent and reliable results. In the case of accidental shifting of the position of the reference electrode, working electrode, and/or counter electrode inside of the cell, impedance and potential readings may become distorted or inaccurate. This is not as important for the preparation cell because the objective of this cell is simply to prepare the reference by partial lithiation and to determine the value of the plateau voltage (typically ~1.565 V for the lithium titanate electrodes used in this procedure).

One good method for determining the success of the cell is through the observation of impedance distortion for the anode. In the case of an improperly sealed cell, or a poor electrode alignment, inductive impedance loops are often seen when taking the anode

impedance. These loops are more easily noticed when the cell is fully discharged, i.e. when the cell is first constructed, so they can be tested for prior to any cycling of the cell. An example of an anode impedance spectra with the distortion present is shown in Figure 21.

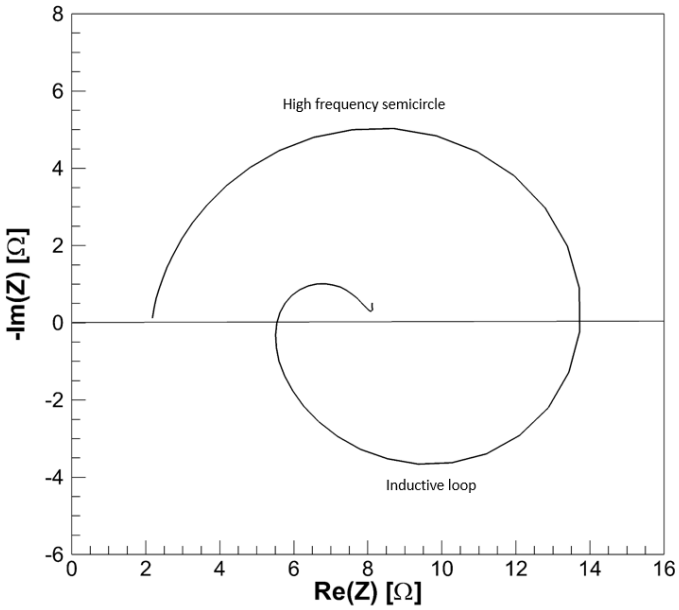

Figure 21. Impedance distortion seen for the anode, likely due to either the cell leaking or a misalignment of the reference electrode

CHAPTER III

ELECTROCHEMICAL CHARACTERIZATION: PERFORMANCE AND ELECTROCHEMICAL IMPEDANCE SPECTROSCOPY

OVERVIEW

The objective of this chapter is to electrochemically characterize electrodes, which can be from any variety of sources, using the three-electrode setup described in the previous chapter. More specifically, the performance (i.e. voltage and potential profiles during cycling) and the electrochemical impedance spectroscopy for the full cell, cathode, and anode are collected. One of the main goals is to use this information to characterize the electrodes in an attempt to detect lithium plating. In addition, another major objective is to allow fast charging of the cell without the occurrence of lithium plating. This will be accomplished using anode based control, which is discussed in the following chapter.

The data collection procedure was organized according to the form factor: coin cell, pouch cell, and 18650 (cylindrical) cell. The schematic of the plan is summarized in Figure 22. The first three topics (configuration, voltage profiles, and impedance) will be covered in this chapter. The final chapter will cover the use of anode-based CCCV control.

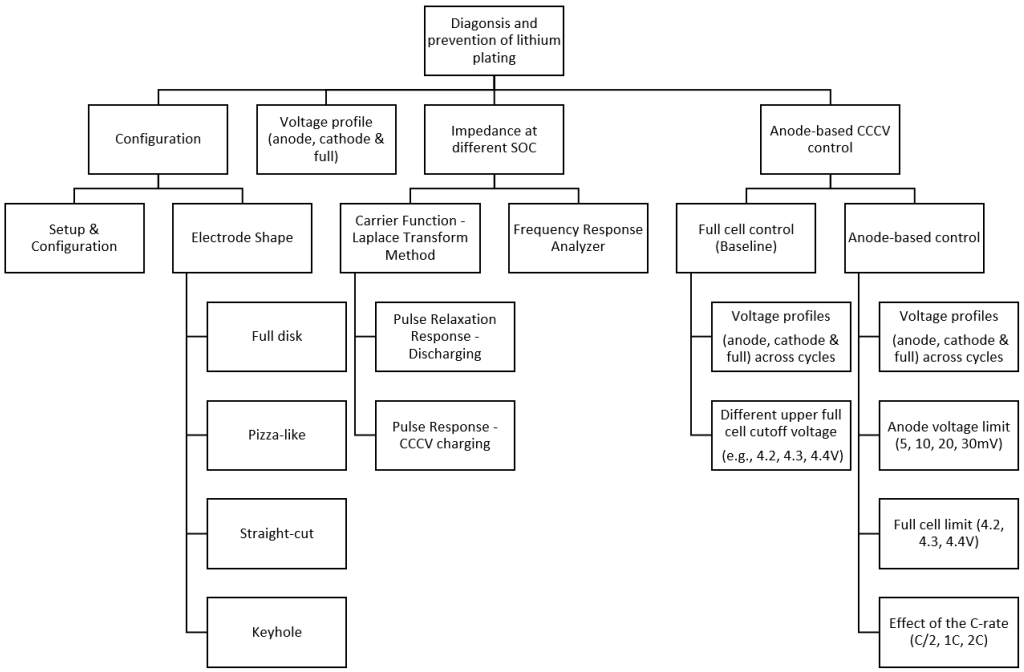

Figure 22. Schematic of electrochemical characterization data collection for development and use of three-electrode coin cell.

EFFECT OF ELECTRODE SHAPE

The first step in the process was to begin the coin cell data collection. One of the first steps was to select an appropriate electrode shape to use. Various electrode shapes were tested and it was found that some of them exhibited impedance distortion and others exhibited inaccurate and/or inconsistent voltage readings. Impedance distortion was seen mainly for the anode measurement and usually took the form of an inductive loop. Inaccurate voltage reading was also seen in some cases for the anode as the voltage reached values far below

zero, which would suggest extreme problems with lithium plating. The problem was that these negative anode potentials were occurring during very low charging rate at room temperature, where lithium plating should not be an issue. Thus, it was determined that the readings were inaccurate. The unwanted distortion and inaccurate voltage readings were used to select the best electrode shape.

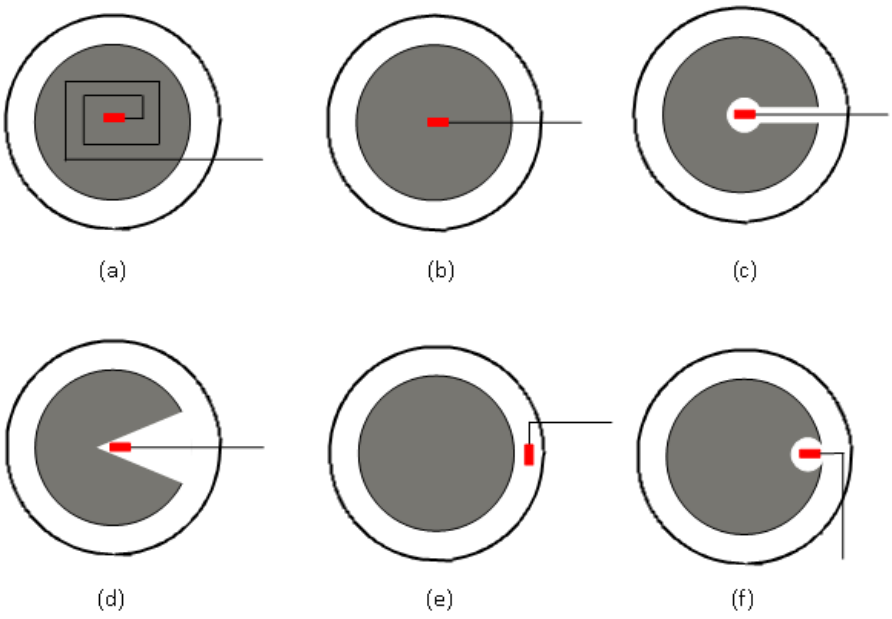

Figure 23. Various possible electrode shapes for three-electrode coin cell

Shown in Figure 23 are several possible electrode shapes which can be used for the three-electrode coin cell setup. The configuration shown in part (a) of the figure is the configuration used for the preparation cell, which has been discussed in the experimental

setup. The configuration shown in part (b) is for the working cell, also discussed in the experimental setup chapter. Configurations (c), (d) and (f) employ an additional cutout section of the electrode. The purpose for this is twofold: (1) to ensure a uniform pressure along the cathode and anode contact area, and (2) to avoid blocking the contact area with the reference electrode itself. Configuration (e) accomplishes the same objective by placing the reference at the side of the electrodes.

Another issue is the accuracy of the voltage readings. The reference electrode should be centralized so that it can read the average potential of the electrodes correctly. The farther away the reference is from the center of the electrodes, the greater the impedance between the reference and electrode of interest. This larger distance is important because it introduces impedance distortion and the larger internal resistance affects the voltage/potential reading. Thus, it is desirable for the reference electrode to be placed at the center. Following this logic, configuration (b) and (c) were prime candidates for the final electrode shape. The impedance and voltage data for the different electrode configurations were tested to determine the effect on the data. The anode potential profile for configuration (b) is shown below in Figure 24.

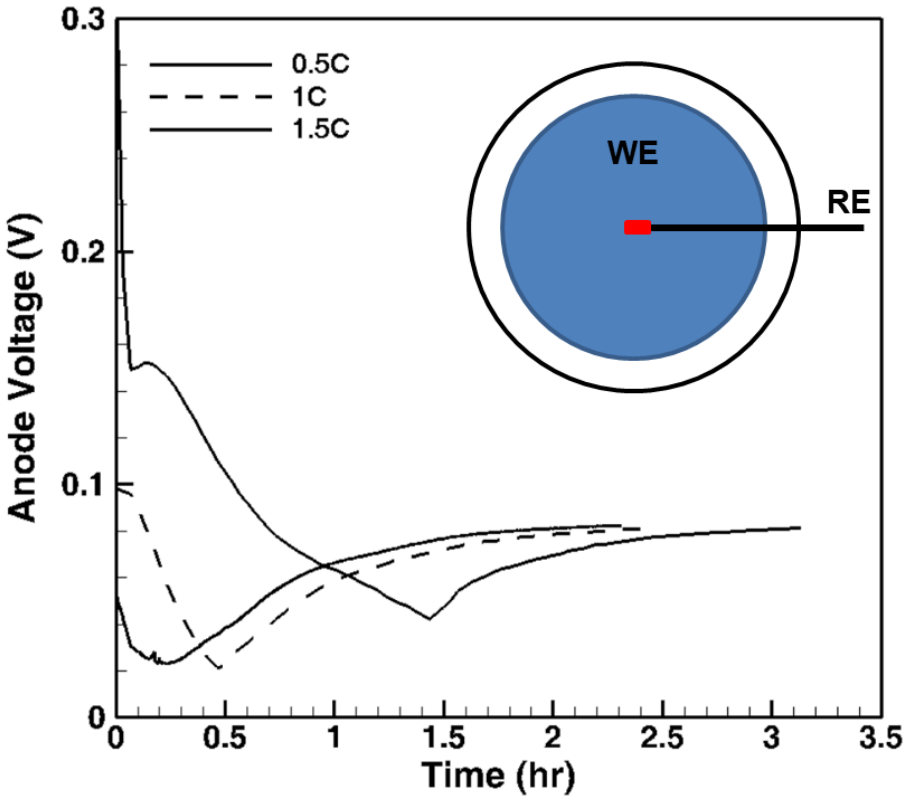

Figure 24. Anode potential during 0.5C, 1C, and 1.5C charging process (CCCV) with full-disk configuration

The cell in Figure 24 corresponds to the full electrode disc and was cycled at various C-rates. For all of the C-rates tested (0.5C, 1C, 1.5C) the anode potential remained positive. This was unexpected due to the host electrodes being specified at a maximum C-rate of 0.7C. Thus, it was determined that the voltage reading was inaccurate. One possible reading for this inaccuracy is the fact that the reference electrode itself is pressed between the two electrode discs (cathode and anode). When the cell is crimped close, there will be

an uneven pressure between the electrode discs; there will be a larger pressure in the center and along the wire due to the lack of space. This non-uniform pressure could lead to a misreading of the potential. The next step then, is to remove the effect of the pressure. This was done by using a keyhole shaped electrode. The results for this configuration are shown in Figure 25.

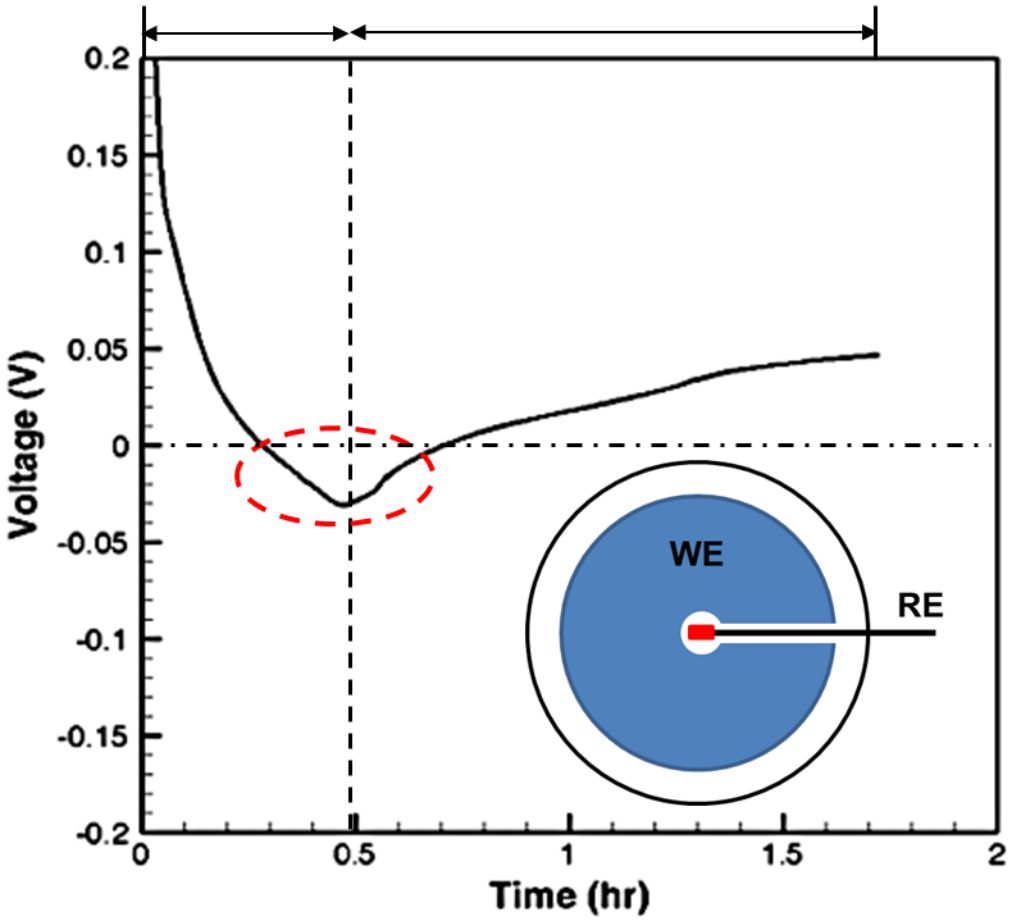

Figure 25. Anode potential during 1C charging process (CCCV) for keyhole configuration cell

Figure 25 shows the anode potential measurement during the charging process for the keyhole configuration. A portion of the potential, circled in red, is below zero during both the constant current (CC) and constant voltage (CV) charging process. The transition from decreasing to increasing potential occurs at the end of the CC and beginning of CV process. The anode potential reaches a negative value as expected, due to the higher C-rate.

The impedance of the electrode configurations was also tested. Shown below in Figure 26 are the results for two of the configurations.

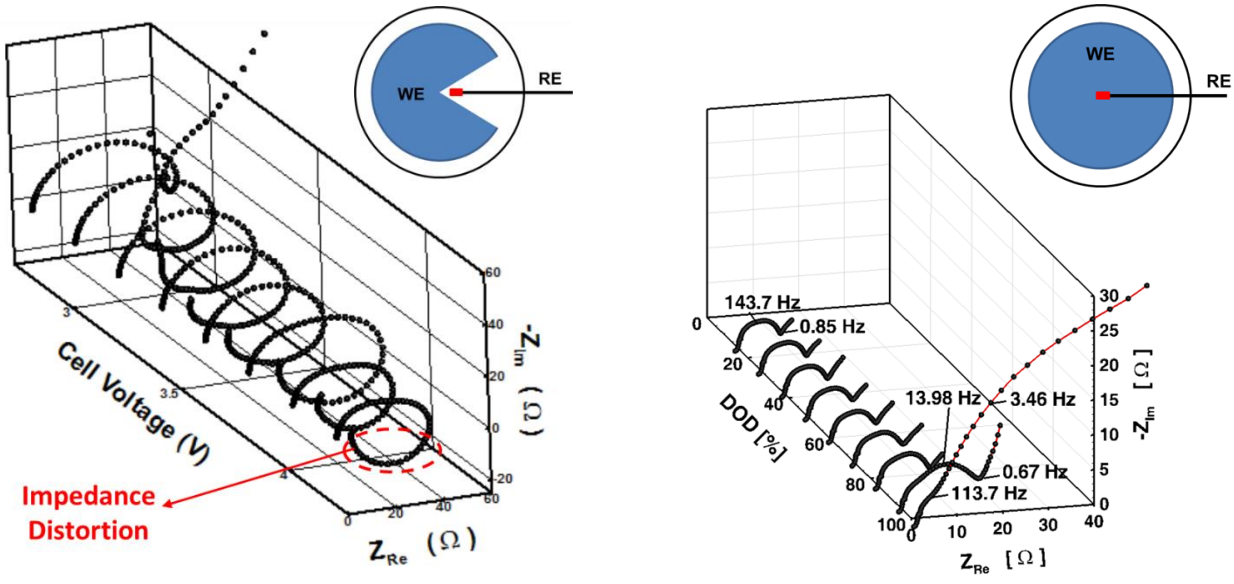

(a) (b)

Figure 26. Anode impedance collected for (a) pizza-like configuration and (b) full disc configuration

The anode impedance for the pizza-like configuration shows a very obvious distortion in the form of an inductive loop. This is likely due to the non-uniformity of the surrounding electrode; the reference is surrounded by material on one side and by electrolyte on the other side. In addition, a misalignment of the cathode and anode discs, for example a slight rotation when making the cell, could cause additional distortion issues. The full disc configuration in Figure 26 (b) shows no signs of distortion. However, as discussed earlier, the potential reading is inaccurate and thus the configuration should not be used for testing purposes.

Other configurations were also tested using the voltage profile and the impedance measurement to determine their reliability and accuracy. A comparison of the electrode shapes can be seen in Figure 27.

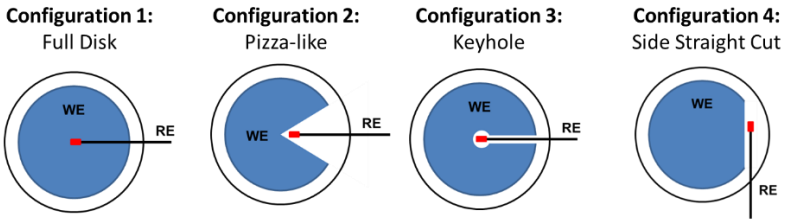

Configuration	1	2	3	4
No Obvious Impedance Distortion	Yes	No	Yes	Yes
Accurate Voltage Reading	No	-	Yes	Yes

Figure 27. Various electrode shape configurations attempted for voltage and impedance measurements

According to the results, the keyhole and side configuration showed no obvious impedance distortion and had accurate voltage readings. Thus, either configuration could be used for the purposes of data collection. The keyhole configuration was selected as the final configuration due to the symmetry and similarity to both the preparation cell and working cell described in the experimental setup. The remainder of the coin cell data can be assumed to have used the keyhole configuration, unless mentioned otherwise.

VOLTAGE AND POTENTIAL PROFILES FOR FULL CELL, CATHODE AND ANODE

After determining the effect of electrode shape on the voltage profile, the next step was to collect representative data corresponding to the full cell, cathode, and anode for the three-electrode coin cell. Three-electrode coin cells were constructed using the keyhole shape and the LTO reference electrode, as described in the experimental setup. The cell was charged at C/10, 1C, and 2C with a voltage window of 2.5-4.2 V. The charging process is of more interest than the discharging process, because this is when lithium plating occurs. Thus, only the charging data is presented. The cell was charged using standard CCCV protocol and the cathode and anode potential were measured simultaneously during testing. The results for the full cell is shown in Figure 28.

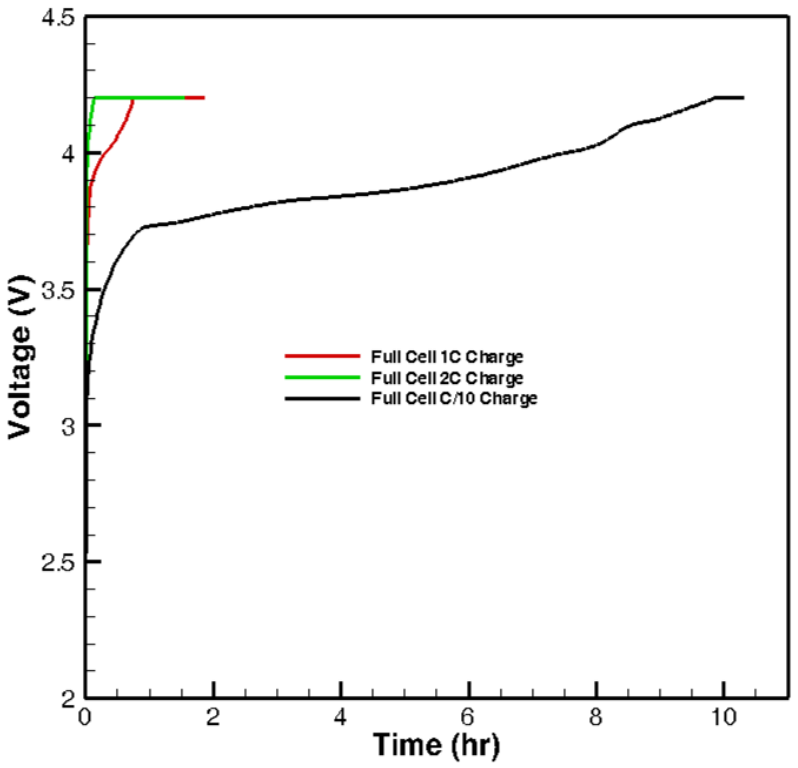

Figure 28. Full cell voltage profile for three-electrode coin cell charged at C/10, 1C, and 2C

From the results presented, the 1C charge took about 0.4 hours for the CC period and a total of 2 hours for the charge to complete. For the 2C charge, the full cell reached the upper voltage limit of 4.2V much more quickly, due to the higher current and the influence of the internal resistance of cell. (Note: the internal resistance of a coin cell is much higher than larger form factors due to the inverse relationship of internal resistance with area). For the C/10 charging, the cell took about 10 hours to charge and included only a very

short CV period, as expected. The cathode potential measurement for the same test is shown in Figure 29.

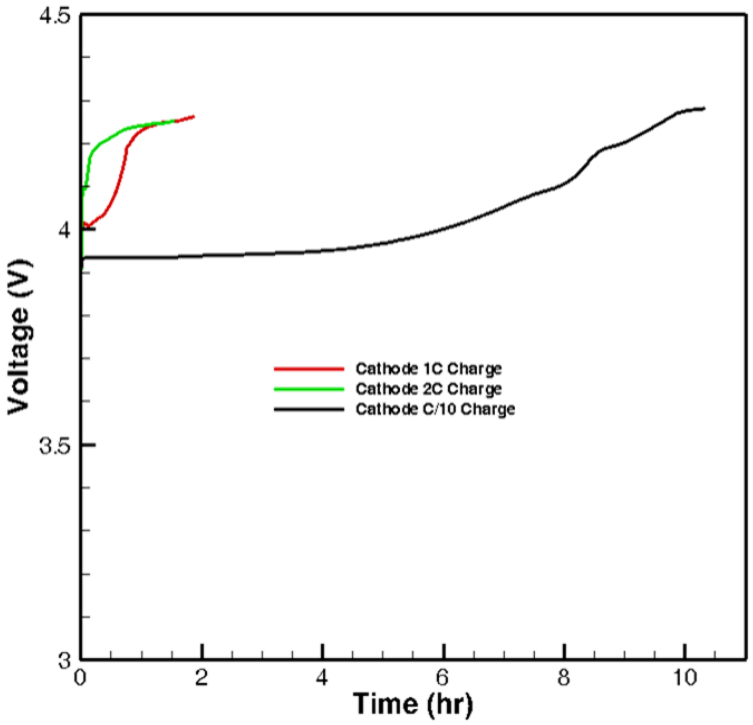

Figure 29. Cathode potential profile for three-electrode coin cell charged at C/10, 1C, and 2C

For the higher C-rates, the cathode potential rises very rapidly and only becomes relatively constant when the cell reaches CV. For the C/10 charging, the cathode potential changes much more smoothly and does not include any semi-flat regions. The anode potential profile for the same test can be seen in Figure 30.

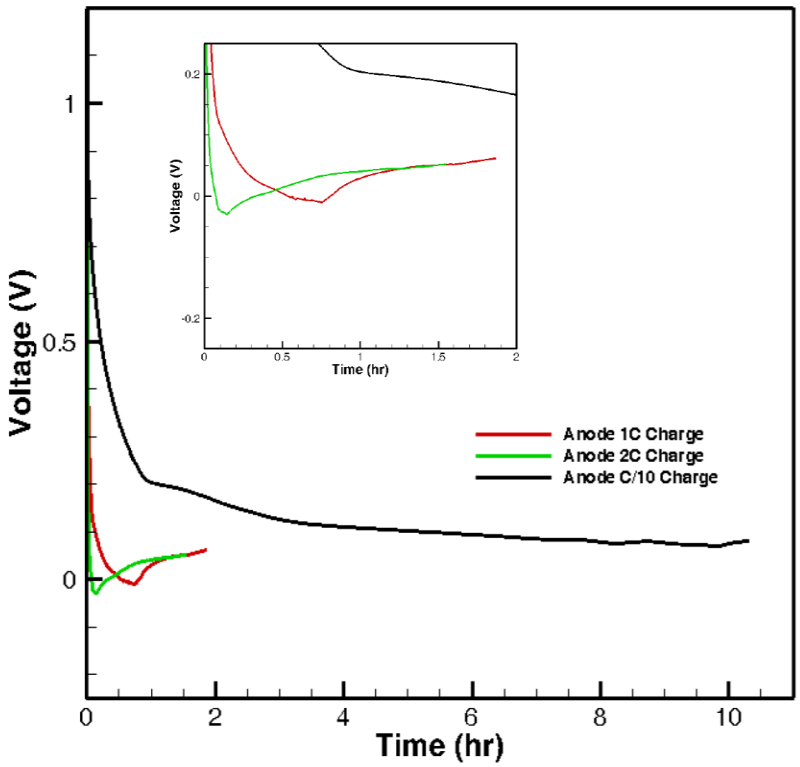

Figure 30. Anode potential profile for three-electrode coin cell charged at C/10, 1C, and 2C

For the anode potential, it can be seen that the value remains above zero during the entirety of the C/10 charging process. This is expected as the low C-rate (C/10) and the temperature (~22°C) would allow for adequate diffusion of the lithium into the anode structure, and thus lithium plating should not be an issue.

For the higher C-rates (1C and 2C) the anode potential does reach negative values. It reaches a minimum value at the end of the CC period and relaxes upwards during the CV

period. Thus, the following important conclusions can be drawn. Lithium plating occurs during fast charging and can be detected in the form of a negative anode potential. This occurs during the end of the CC charging period and the beginning of the CV charging period.

ELECTROCHEMICAL IMPEDANCE SPECROSCOPY AS A FUNCTION OF STATE OF CHARGE

After successfully detecting the existence of lithium plating by measuring the negative anode potential during fast charging, the next step was to characterize the impedance of the full cell, cathode and anode as a function of the cell state of charge (SOC). Note that this is only possible with the use of a three-electrode cell. Two different methods to collect the impedance as a function of the state of charge are the use of a Frequency Response Analyzer (FRA) and the use of the Laplace Transform Method (LTM). The Frequency Response Analyzer will be discussed first.

A frequency response analyzer is an experimental instrument used to measure properties in the frequency domain. In this case, it was used to measure the electrochemical impedance spectroscopy of the three-electrode coin cell. A Biologic VMP3 potentiostat system was used for this data collection. The potentiostat system is shown in Figure 31 and the connection to the three-electrode coin cell is shown in Figure 32.

Figure 31. Biologic VMP3 potentiostat system used in the collection of electrochemical impedance spectroscopy

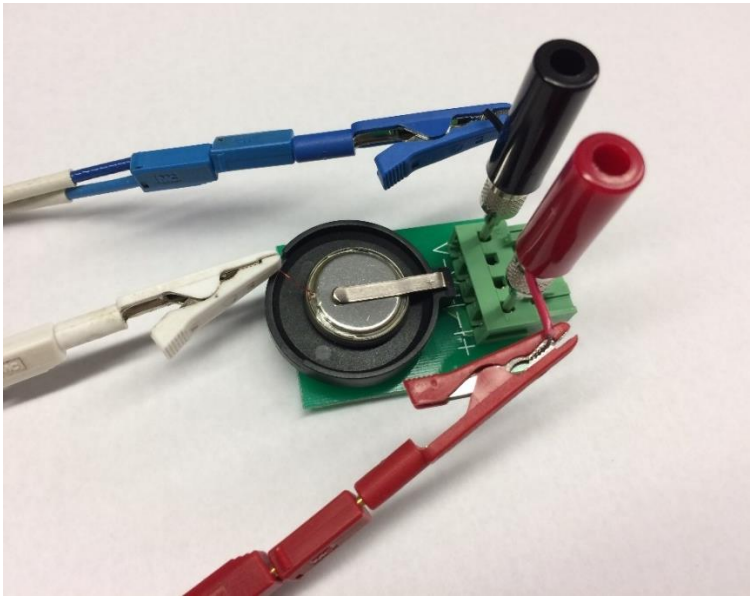

Figure 32. Photograph of three-electrode cell connection to the potentiostat system. Note that this connection is specific for cathode impedance measurements (refer to Figure 19).

The FRA works by applying either a galvanostatic (current based) or potentiostatic (voltage based) sinusoidal excitation function to the experimental system. It then measures either the current or voltage response back (i.e. it is not possible to control both the current and voltage at the same time). It uses the ratio of the current and voltage to calculate the impedance of the cell as a function of the frequency. For the data collected herein, potentiostatic EIS was implemented.

Two main parameters for the potentiostatic FRA are the frequency range and the voltage amplitude. The frequency range will not change the results and should only be tuned for the specific area of interest. Having a very large frequency range will only increase the time of the test and collect superfluous data. The voltage amplitude should be small enough to provide a detectable response in the cell but not so large as to actually change the cell's SOC significantly. If the voltage amplitude is too large the cell will not be stable and the response will not be representative of the open circuit voltage of the cell (OCV) or open circuit potential (OCP) of the cathode/anode. For the FRA data presented here, the frequency range was selected from 10 KHz to 13 mHz and the voltage amplitude was set at 10mV. These values are based on trial and error testing of multiple cells in search of a repeatable and accurate results.

In order to collect EIS as a function of SOC, the cell SOC needs to be changed. For this data collection, a protocol was setup with the Biologic VMP3 system. A flowchart of the process is shown in Figure 33.

The protocol consists of three subsections: the preparation (green), the CC charging loop (red) and the final measurement (yellow). In a general sense, what the protocol does is charge the cell at C/10 for 1 hour (hence changing the SOC by 10%), collect the impedance, and loop. Thus, the final result should be a set of 10 impedance spectra in multiples of 10% SOC. The preparation portion simply makes sure that the cell is always starting from the fully discharged (0% SOC) state. The CC charging loop simply includes a looping CC charging and impedance collection. Once the cell is fully charged, a single measurement is taken (100% SOC) to finish off the data.

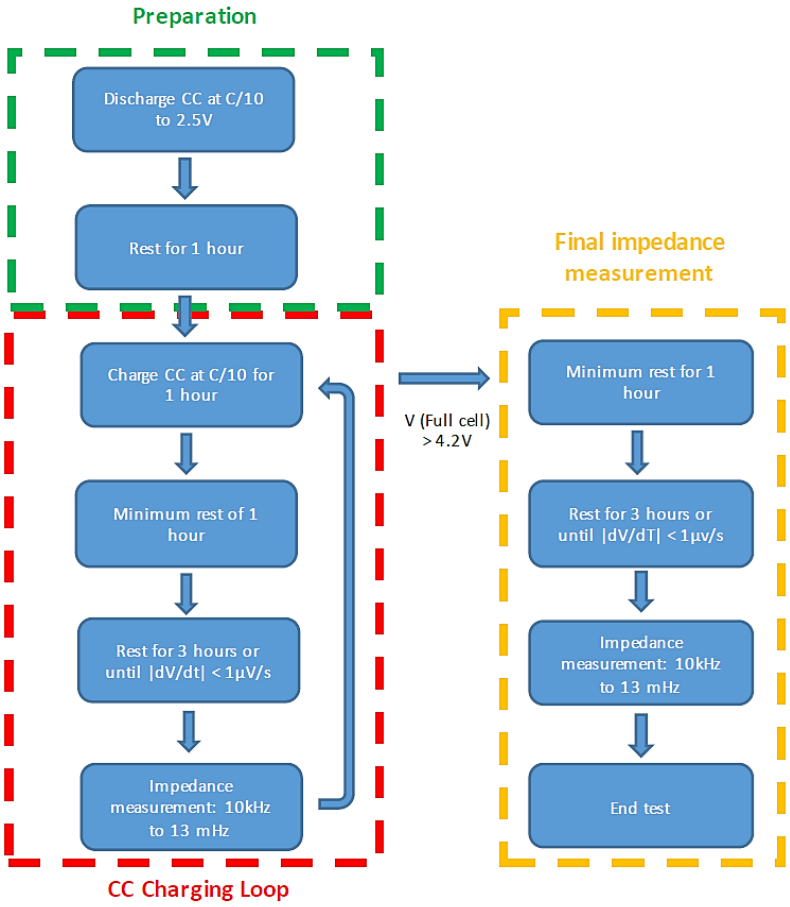

Figure 33. Flowchart for impedance as a function of SOC collected by Frequency Response Analyzer

The protocol was implemented on the frequency response analyzer and the impedance was collected. Note that using this protocol, it is only possible to collect one set of impedance per run. Thus, the test was run a total of 3 times to collect the full cell, cathode, and anode impedance. The FRA data for the full cell, cathode, and anode can be seen in Figure 34, Figure 35, and Figure 36, respectively.

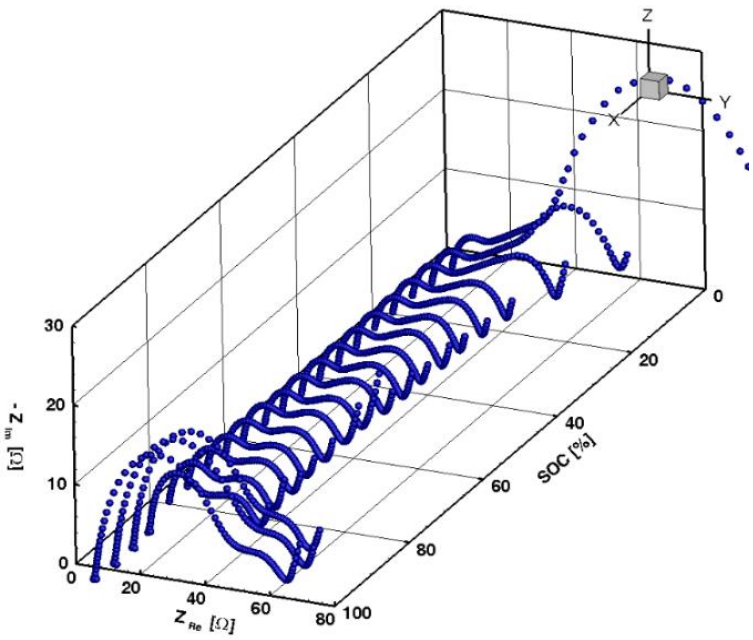

Figure 34. Full cell impedance for keyhole configuration collected using the FRA

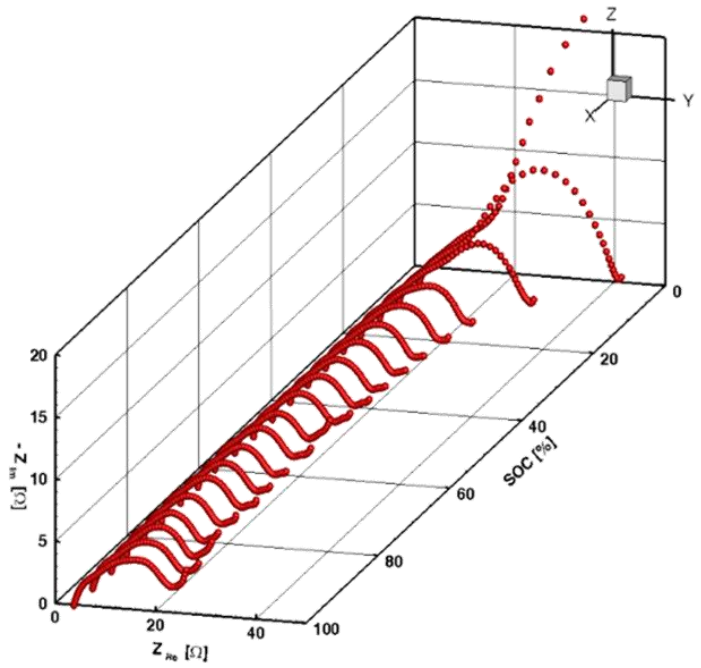

Figure 35. Cathode impedance for keyhole configuration collected using the FRA

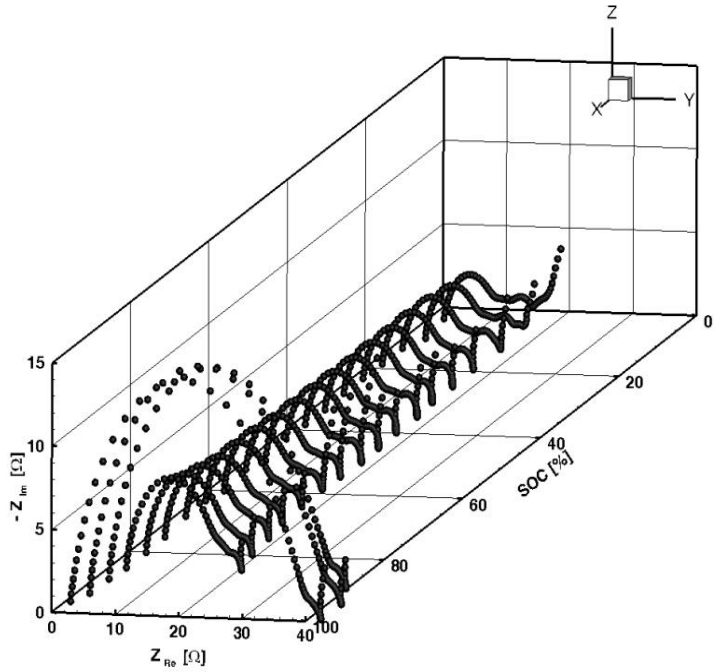

Figure 36. Anode impedance for keyhole configuration collected using the FRA

From the full cell impedance, it can be seen that the full cell has larger impedance values at both 100% SOC and 0% SOC. In a standard two electrode cell, an explanation of this might be difficult from the given data. In order to elucidate the causes of this, it is beneficial to look at the cathode and anode impedance spectra.

The cathode displays very high impedance at low SOC while the anode displays high impedance at high SOC. This can be explained using the fundamental processes which occur inside of the battery. At high SOC the anode electrode is almost entirely full of lithium. In trying to store more lithium in the structure, there will be a very high impedance, corresponding to the lack of space. The same is true for the cathode at low

SOC. At low SOC most of the lithium is stored in the cathode, and thus the higher impedance can be attributed to the lack of space in the structure to store more lithium.

After understanding why the cathode and anode show high impedance at their respective SOC, the full cell response can be explained. At low SOC, the anode impedance becomes very large and dominates the system, and thus the full cell also has a large impedance. At high SOC, the cathode impedance becomes large and dominates the system and thus the full cell has a larger impedance at this SOC as well. In the middle range of SOC, the impedances of both the cathode and anode become stable and thus the full cell also shows a relatively stable impedance with not much changing across the SOC.

A second method to collect EIS data for the three-electrode coin cell is the Laplace Transform Method. The basis of the LTM is a conversion between time and frequency domain. High frequency pulse data is collected using an electrochemical testing machine. This data is then run through a code which implements the LTM and converts the data to frequency domain.

The pulse data collection was implemented also on the Biologic VMP3 potentiostat. The protocol can be seen in Figure 37. There are two main loops: a CC and CV charging loop. For the CC charging, there is a nominal charging rate (1C) which occurs most of the time. During the pulse periods, there is either an upper pulse (1.1C) or a lower pulse (0.9C). These C-rates are arbitrary and can be changed as required. In addition, there is high frequency data collection during and immediately after the pulse and lower frequency data collection for a longer period after the pulse. The LTM uses the current and voltage which

occurs during and after the pulse to calculate the EIS for the system. The amount of charge passed during the test can be used to determine the state of the charge of the cell.

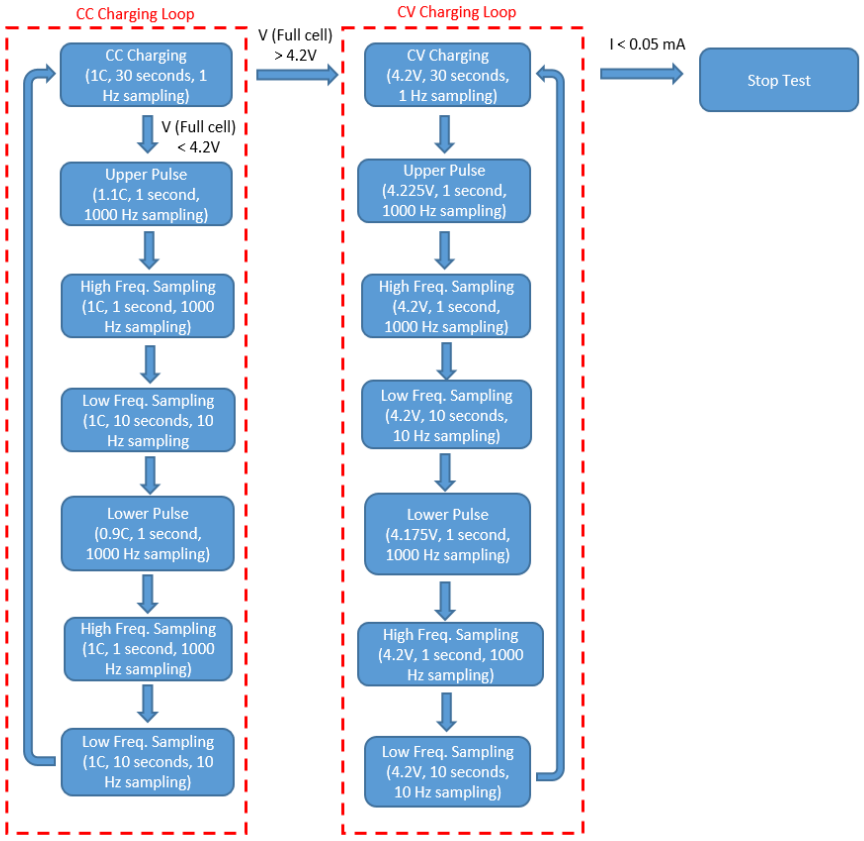

Figure 37. Pulse data collection to be used with Laplace Transform Method for electrochemical impedance spectroscopy

The pulse data which corresponds to the protocol presented in Figure 37 can be seen in Figure 38 and Figure 39 for the full cell and cathode and anode, respectively.

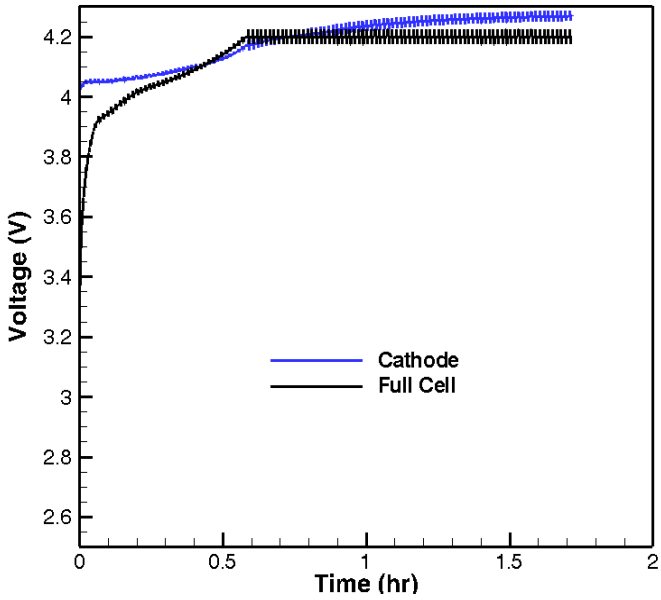

Figure 38. Laplace Transform Method pulse data collected for full cell and cathode

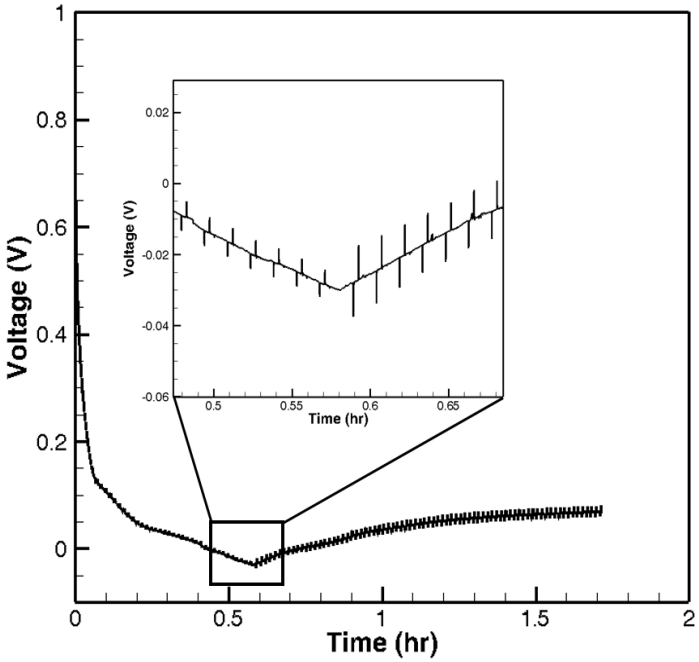

Figure 39. Laplace Transform method pulse data collected for anode

The voltage/potential for the full cell and cathode are as expected. The voltage limit of the full cell is set from 2.5-4.2V. The voltage peaks can be easily seen in the plot which corresponds to the upper and reduced pulses. The CV peaks are larger than the CC peaks and are constant because they are set based on a voltage, and not a C-rate like the CC pulses. The anode potential profile can be seen in Figure 39. One important note is that the anode potential reaches negative value during the charging process. This is likely because the nominal rate is 1C, which was found to exhibit negative anode potential during normal charging (see Figure 30).

A close-up of the voltage pulses themselves was also analyzed. These can be seen in Figure 40 for the full cell and Figure 41 for the cathode and anode.

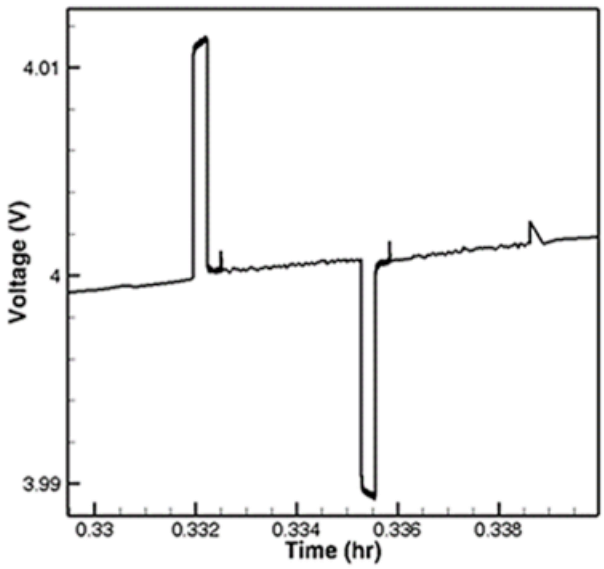

Figure 40. Full cell pulse corresponding to LTM pulse charging protocol

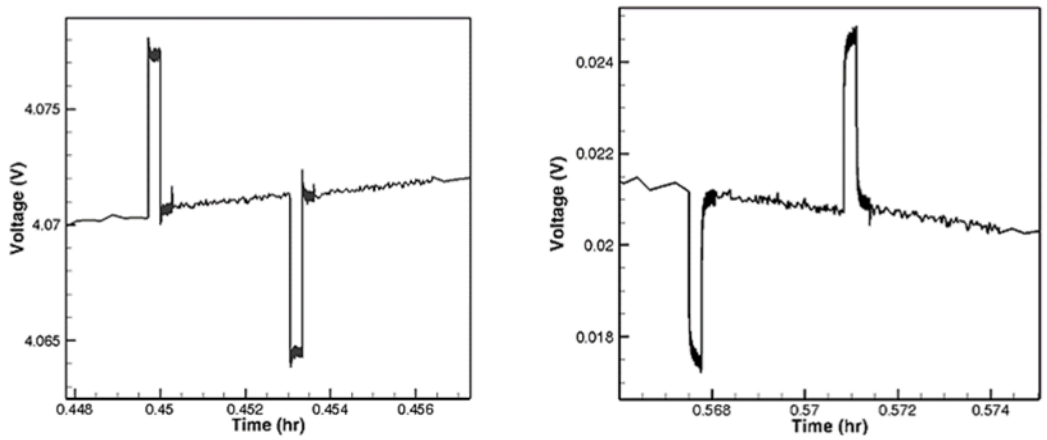

(a) (b)

Figure 41. (a) Cathode and (b) anode pulse corresponding to LTM pulse charging protocol

Upon looking at the full cell, cathode, and anode pulses, one observation is that the cathode and anode pulses show more fluctuation during the high frequency data collection which occurs both during and after the pulse is applied. This is likely due to the reference electrode. The additional fluctuations could be due to the movement of the reference electrode inside of the cell during the testing procedure.

In order to convert this pulse data into impedance data, a code must be developed which utilizes the LTM and the pulse data. At this point the code is still being developed and thus the EIS data is not currently available for these specific results. The development of this code will form part of the suggestions for future work and improvements.

There is a subtle distinction between the FRA and LTM strategies for impedance characterization. Although it might be thought that in a perfect world the two impedances should show the same response, this is not the case. The FRA impedance is taken at open circuit conditions, after the cell has been resting and the voltage change with respect to time is below a certain threshold value. The LTM impedance is taken *insitu* during the charging process. Note that for the LTM pulse protocol the cell is never resting and all of the data is collecting during operation. Thus, the LTM data is collected *in-operando.* Because both methods are measuring impedance in a slightly different manner, they can be used in conjunction with each other to understand different aspects of the electrochemical system or battery.

CHAPTER IV

ANODE POTENTIAL BASED CCCV CONTROL

OVERVIEW

The goal of this section of research was to prevent lithium plating, using the knowledge acquired from the previous characterization data. From the previous data, it was found that lithium plating can be detected when the anode potential reaches values below zero with respect to Li/Li^+. The anode potential can be measured directly using the three-electrode cell described in Chapter II. Thus, this section combines the knowledge learned in Chapters II and III and utilizes it to improve the performance of lithium-ion cells in experimental operation.

In order to prevent lithium plating, the anode potential must not be allowed to reach values below 0 V (with respect to Li/Li^+). In a standard two-electrode cell this is impossible because the anode potential cannot be known directly, only the full cell. The introduction of the three-electrode allows this protocol to run due to the direct measurement of anode potential. In fact, without this three-electrode setup, this anode potential based control would not be possible.

Standard batteries are charged using a constant-current constant-voltage protocol. The idea is that the cell is first charged using a constant current while the cell voltage is monitored. After the cell reaches a specified upper voltage, the constant voltage protocol is started. At that point, the cell voltage is held constant while the current is monitored. Once the current drops below a certain (arbitrary) value, the cell is said to be fully charged.

One of the main problems with standard CCCV charging is that there is a limit to how fast it can be conducted. At very high charging rates degradation can become a huge issue as lithium can plate onto the anode surface. This causes a reduction in cell capacity as well as safety issues if the lithium grows to pierce the separator.

Anode CCCV control can alleviate this issue as the anode potential itself can be used as a control variable. Instead of charging the full cell to 4.2 V, the cell can be charged until the anode reaches a value slightly above zero, 10mV for example, and held with a constant anode potential to charge the cell. This ensures that the anode potential never drops below zero and thus plating is never an issue. This control strategy can be accomplished using a three-electrode setup as the anode potential is known at all times.

One important distinction is that in both methods the cell is being charged across the full cell. For the anode control, the anode itself is not being charged, the full cell is, and the anode potential measurement is only being used as a control variable. This is important to understand as there is never any current passed through the reference electrode. A summary of the differences can be seen below in Figure 42.

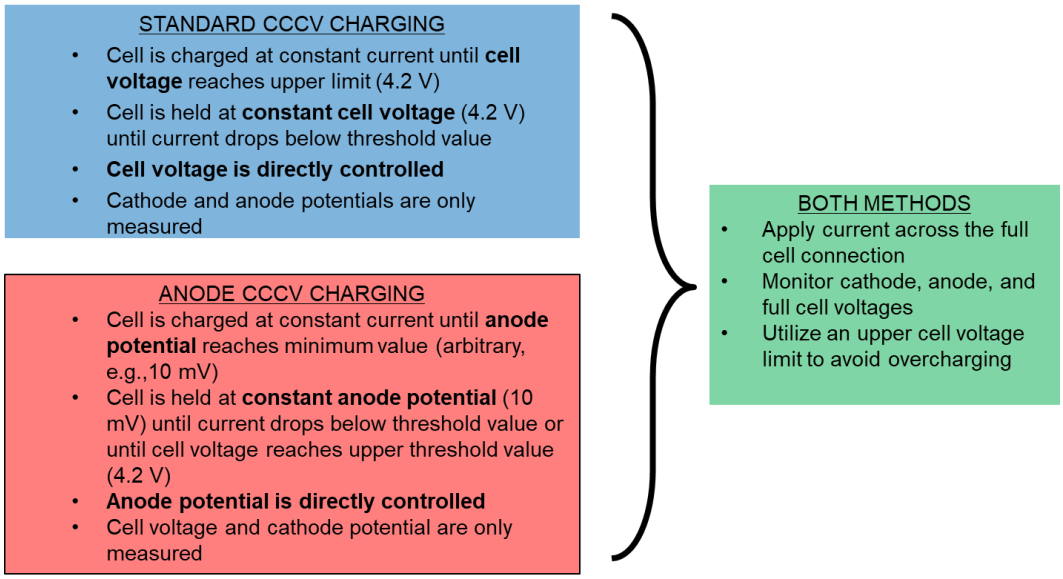

Figure 42. Comparison between standard CCCV and anode CCCV charging protocols

PROTOCOL

The anode control method is based on using the anode potential as the control variable. Because of this fact, it is possible for the cell to become overcharged as the full cell voltage is not directly controlled. Because of this, there are two main control parameters which were implemented: the lower anode potential limit and the upper full cell limit. If the full cell went above a specific limit (4.2 V for example) the cell would stop charging to ensure overcharge did not occur. This is important because as the cathode potential increases other degradation phenomena can occur. A schematic of the anode control protocol can be seen below in Figure 43.

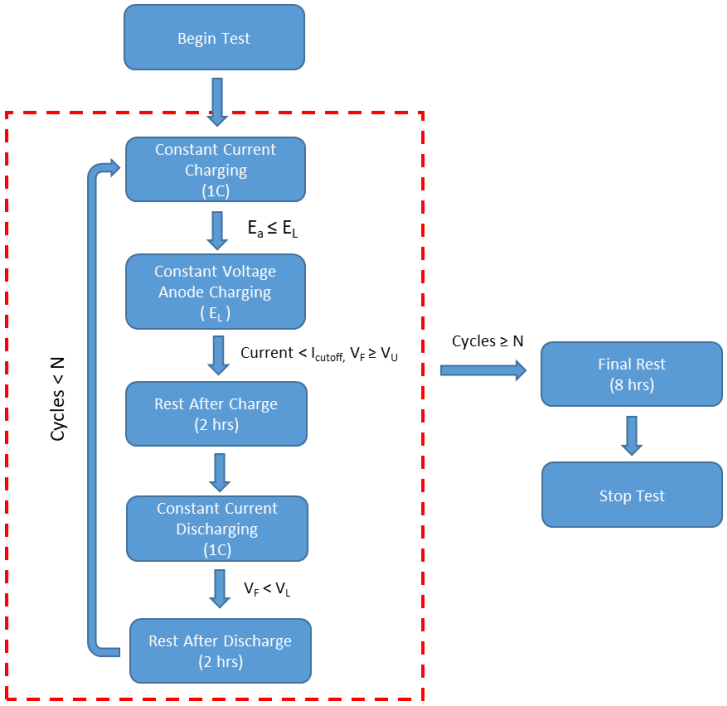

Figure 43. Flowchart for anode control protocol

In the figure: E_a is the anode potential, E_L is the lower anode potential limit, I_{cutoff} is the CV cutoff current, V_F is the full cell voltage, V_U is the upper full cell limit, V_L is the lower full cell limit, and N is the total numbers of cycles desired.

The protocol uses a combination of the anode potential and full cell voltage as limits in the charging process and only the full cell limit during the discharging process. This is because plating is only an issue during the charging process and thus the anode potential is unimportant during discharge.

RESULTS

Because the protocol allows different upper full cell limits, it was important to collect baseline data using a standard CCCV protocol. This is important because a higher full cell limit will correlate with a higher capacity. Thus, it is important to have separate baseline cells for each upper full cell limit. For this work, it was decided to use upper full cell limits of 4.2V, 4.3V, and 4.4V.

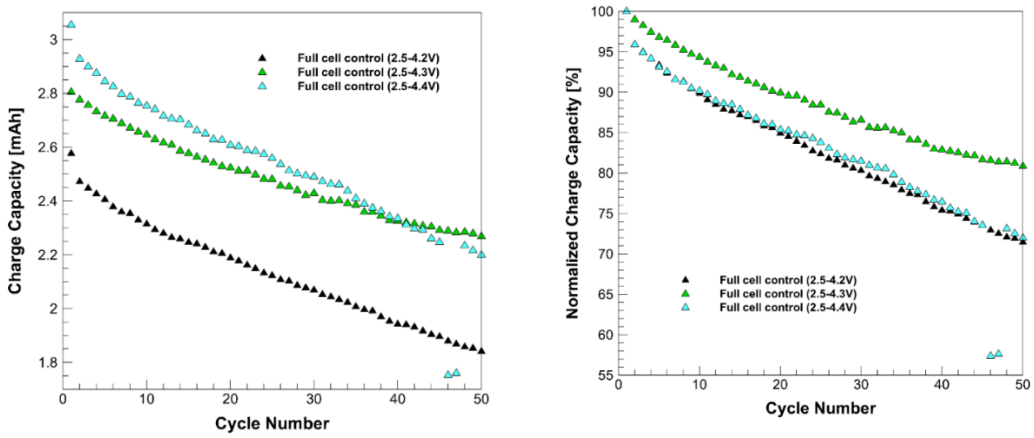

(a) (b)

Figure 44. Full cell cycling data for (a) charge capacity and (b) normalized charged capacity, with different upper full cell limits, to be used as baseline for anode potential control

These values were selected based on the maximum value achieved during the anode potential control tests. Also, increasing the upper full cell limit too high could cause degradation to occur in the cathode, which is not the focus of this study and thus is undesirable. The performance of the full cell baseline cells across 50 cycles is shown in Figure 44.

From the figure, it can be seen that the higher voltage limit corresponds to a higher charge capacity, as expected. The 4.4V upper limit had the highest initial capacity, the 4.3V had the middle capacity, and the 4.2V had the lowest capacity. An important observation though, is that as the cells cycle, the rate of capacity decrease is not the same. Towards the end of the 50 cycles, the normalized capacity plot shows that the normalized capacity retention of the 4.3V cell exceeds that of the 4.4 V. This could be due to additional degradation occurring at the cathode or in the electrolyte due to the existence of a higher cell voltage. During the test, the anode potential was monitored to see what would happen if no anode control was implemented. The charging rate for all of the tests was 1C. This data is shown in Figure 45.

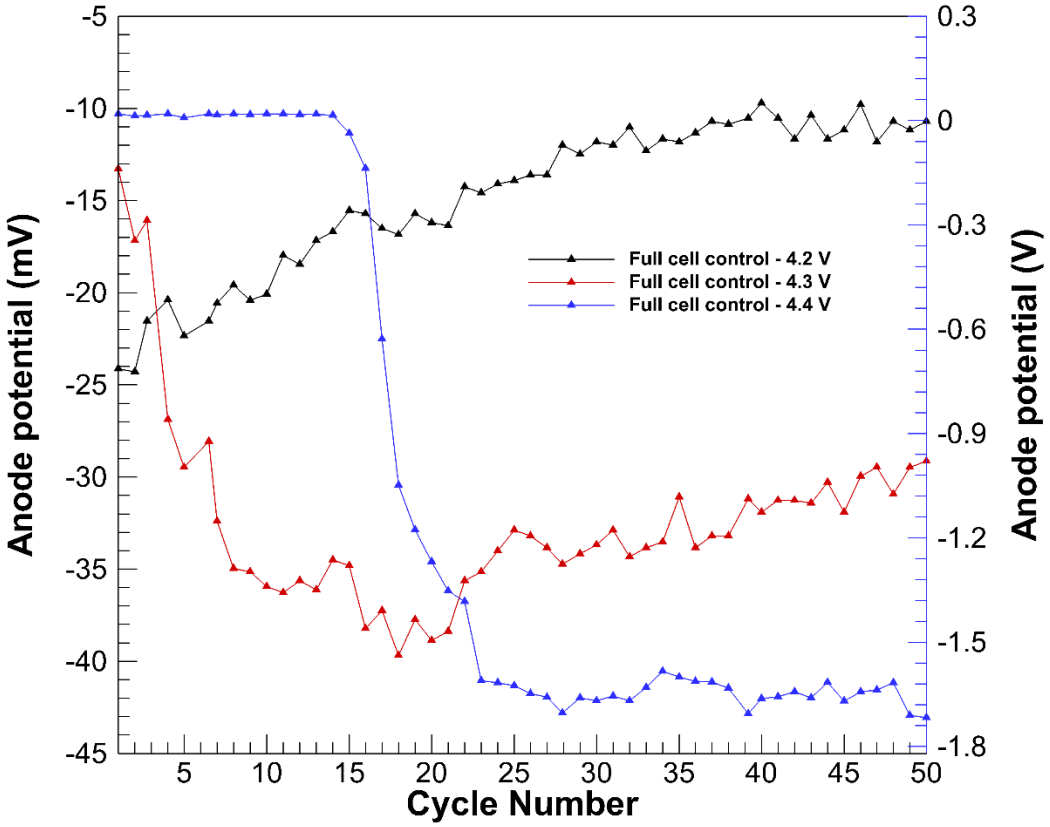

Figure 45. Minimum anode potential measured for full cell control method, charging at 1C

The minimum anode potential shows some interesting trends. In all cases, the anode potential reached negative values and thus plating was an issue. The highest upper cell limit (4.4V) showed a much lower anode potential, as expected. The qualitative trends for all three cells were different. The 4.2V cell showed a generally increasing anode potential. One hypothesis for this might be that the plating occurred early on in the cycling process

and the overall capacity of lithium decreased. As the lithium inventory was lowered, there was plenty of space inside the anode structure to store the remaining lithium and thus the plating (and negative anode potential) reduced.

The 4.3V upper limit cell shows a decrease and then increase in the anode potential. Once hypothesis is that this is due to the tradeoff between the SEI growth and lithium plating. Initially the growth of the SEI is important and thus the internal resistance of the cell increases. This increase in resistance causes a lower potential due to the ohmic drop in the cell. After the SEI growth has slowed down, the effect of plating over many cycles reduces the internal resistance of the cell. This leads to a higher anode potential as the number of cycles increases. This might explain the behavior of the 4.3V cell.

The first test involved using an anode control of 10mV and an upper full cell limit of 4.2 V. These results are then compared to the full cell baseline (with an upper cell limit of 4.2V). The results can be seen in Figure 46.

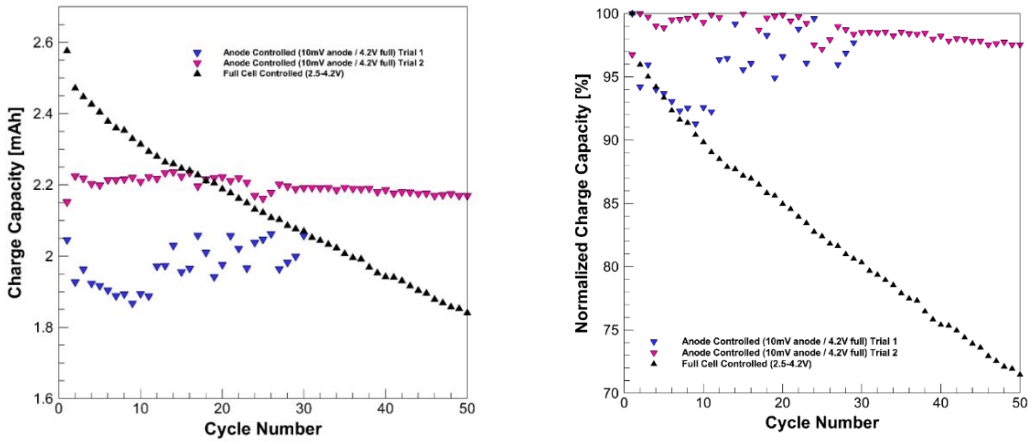

(a) (b)

Figure 46. Anode potential control with 10mV lower anode limit and 4.2V full cell limit, showing (a) charge capacity and (b) normalized charge capacity retention

The baseline full cell control response shows a monotonic decreasing trend in capacity, as seen previously. The two anode control trials show a much difference response. First of all, the nominal capacity achieved by the anode control tests is much lower. This is likely due to the fact that the trial 1 cell reached the upper cell limit of 4.2V and skipped the CV portion of the protocol. This is why the capacity is much lower and the capacity retention fluctuates wildly between 90 and 100% capacity. The trial 2 shows a similar trend except in that the cell is completing a part of the CV charging process, but not the entire step.

After seeing the issues associated with having the upper full cell limit be reached, it was increased to 4.3V while maintaining the same anode potential of 10 mV. The cells were cycled in an identical fashion and the results are shown in Figure 47.

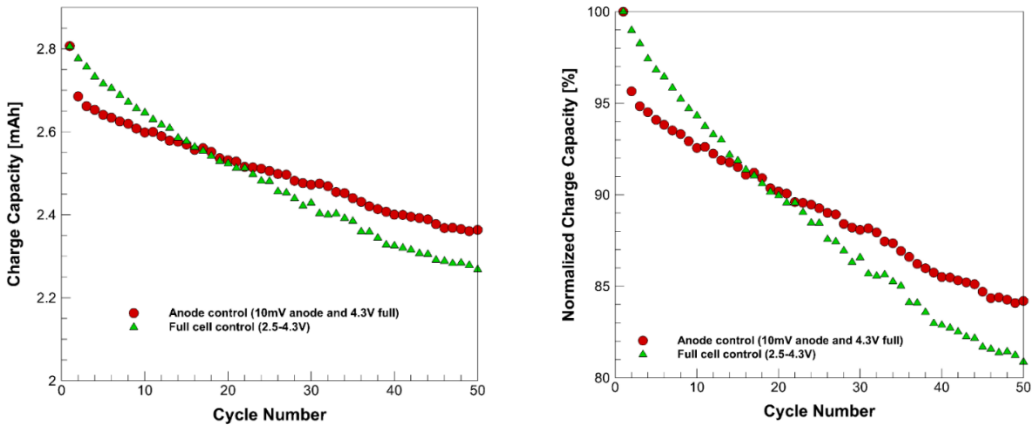

(a) (b)

Figure 47. Anode potential control with 10mV lower anode limit and 4.3V full cell limit, showing (a) charge capacity and (b) normalized charge capacity retention

When the upper cell limit is not reached during each cycle, the capacity retention plots show a much different story. From Figure 47 it can be seen that the anode control has comparable capacity to the full cell control upon the initial cycles. After the cells are cycled, the full cell control capacity drops at a much faster rate than the anode control cell. After 50 cycles, the anode control cell has a better nominal and normalized capacity retention. This is because there is no plating occurring for the anode control cell and there is plating occurring for the full cell controlled cell.

Finally, the minimum anode potential value was decreased to 5mV and the upper full cell was increased to 4.4V to compensate. The cells were cycled again for 50 cycles and the results are shown in Figure 48.

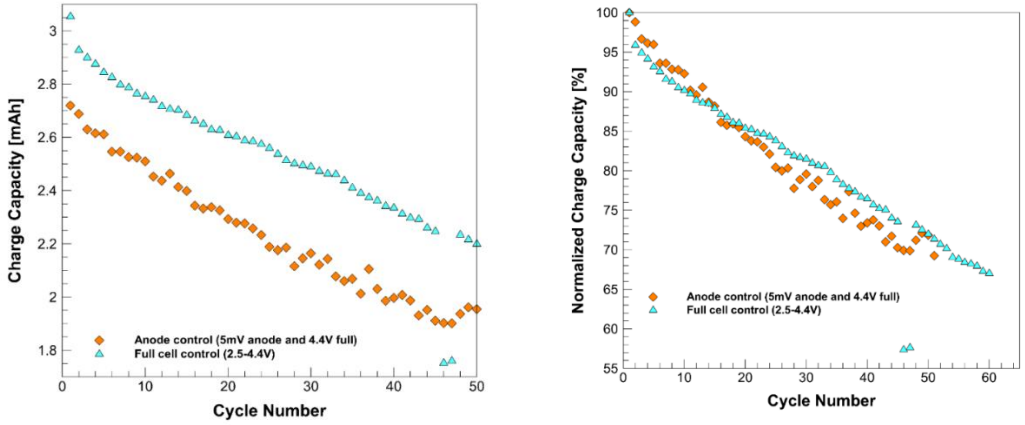

(a) (b)

Figure 48. Anode potential control with 5mV lower anode limit and 4.4V full cell limit, showing (a) charge capacity and (b) normalized charge capacity retention

From the nominal charge capacity, it appears the full cell performs better than the anode control cell. This might be due to the fact that the full cell is held at 4.4V with constant voltage while the anode control cell only reaches a lower value. In addition, the anode control and full cell control show a similar normalized capacity retention behavior. This might be due to the fact that the full cell voltage is increased to such a high number. Increasing the full cell voltage (while maintaining a specific anode potential) will increase the cathode potential. This increase in cathode potential may be causing more capacity

loss than the lack of lithium plating is prevention. Thus, there is a tradeoff between reducing lithium plating by limiting the anode potential and allowing other degradation phenomena to occur at the cathode and in the electrolyte by increasing the upper full cell limit.

In general, the anode control is successful in reducing lithium plating at the anode and increasing the cell capacity retention. This is most obvious for the 10 mV anode limit and the 4.3V full cell limit. In this case both the nominal and normalized capacity retention show a remarkable improvement over the full cell controlled case. In other cases, it is important to be wary of allowing the full cell voltage to increase too much that other degradation in the cathode take place and also for not letting the cell fully charge due to limiting the full cell limit to too low of a value. Thus, a fine balance is required to optimize the cell performance and reduce the lithium plating which occurs.

CHAPTER V

CONCLUSIONS AND FUTURE RECOMMENDATIONS

The overall objective of this work was to diagnosis and prevent lithium plating. The diagnosis was done through a combination of different electrochemical testing methods, including voltage and potential measurements as well as electrochemical impedance spectroscopy. The key to this degradation characterization was the use of an experimental three-electrode cell setup, which allowed the direct measurement of the cathode and anode potentials in addition to the full cell voltage. This also allowed the contribution of the cathode and anode impedance to the full cell response to be better understood. Neither the electrode potentials nor the individual electrode impedance could be collected without the development and optimization of this three-electrode setup.

The voltage and potential measurements collected by the three-electrode setup allowed for better understanding of the fundamental processes involved. More specifically, the anode potential was used to detect when lithium plating was occurring. When the anode potential went below 0V vs Li/Li^+, lithium plating occurred. It was confirmed that lithium plating occurred only at high C-rates (1C, 2C) and not at low C-rates (C/10). All of the tests performed were conducted at room temperature (~22 °C). Lithium plating becomes more severe at low temperature due to the reduced solid state diffusion in the electrode structure. These low temperature tests could prove valuable and are left as a future work.

The impedance characterization was collected using two different methods. One method used an experimental Frequency Response Analyzer (FRA) while the other relied on the

Laplace Transform Method (LTM). The FRA impedance showed that at low cell states of charge (SOC) the cathode impedance dominated while at high states of charge the anode impedance dominated. This explains why the full cell shows higher impedance at either 100% or 0% SOC, and a more moderate impedance in the middle range. The high impedance of the anode at high SOC is one example of why lithium plating predominantly occurs during the end of charge (and thus at high SOC).

Pulse data was also collected to be used with the LTM. The data included charging the cell at a nominal C-rate and including upper and lower pulses. During this process the cell was continuously charged, albeit at different C-rates. This data has been collected and is ready for conversion using the LTM. The development and use of a code which can convert the data produced by this specific pulse protocol forms a good area for future work.

Finally, anode potential based control was used to prevent lithium plating and improve capacity retention over numerous cycles. Both the anode potential limit and the full cell limit were used together to improve the cell response. The results showed that increasing the upper cell voltage too high is detrimental, possibly because it allows other degradation phenomena to occur at the cathode and for the full cell to become overcharged. Limiting the anode potential too much caused the cell to not become fully charged. This shows up as great capacity retention but poor nominal capacity values.

In terms of future work, there is a lot that can still be done. One idea is to work on the development of an equivalent circuit model which incorporates the effect of lithium

plating. This would be a strong addition to the work presented here. The circuit could be used to fit experimental impedance data and determine the influence of plating on the cell response. This might even be able to quantify numerically some of the factors related to plating, for example: mass of lithium plated or change in cell impedance due solely to the plating.

In addition, some optimization could be done with the anode potential CCCV control. What was presented here was a first step towards understanding the best method to use. The anode control method is particularly useful when considering fast charging of cells, and thus taking a more detailed look into the effect of the C-rate could prove valuable. This would help save time when charging battery systems while simultaneously avoiding the drawbacks associated with lithium plating.

Understanding degradation phenomena in lithium-ion batteries is very important because it leads the way towards better safety and better performance. The three-electrode cell is a very powerful tool which can be used to provide an incredibly detailed look into the many complicated and coupled processes occurring inside of a battery system.

REFERENCES

[1] B. Dunn, H. Kamath, and J. M. Tarascon, "Electrical Energy Storage for the Grid: A Battery of Choices," (in English), *Science,* vol. 334, no. 6058, pp. 928-935, Nov 18 2011.

[2] P. G. Bruce, B. Scrosati, and J. M. Tarascon, "Nanomaterials for rechargeable lithium batteries," (in English), *Angewandte Chemie-International Edition,* vol. 47, no. 16, pp. 2930-2946, 2008.

[3] J. B. Goodenough and Y. Kim, "Challenges for Rechargeable Li Batteries," (in English), *Chemistry of Materials,* vol. 22, no. 3, pp. 587-603, Feb 9 2010.

[4] B. Scrosati and J. Garche, "Lithium batteries: Status, prospects and future," (in English), *Journal of Power Sources,* vol. 195, no. 9, pp. 2419-2430, May 1 2010.

[5] J. M. Tarascon and M. Armand, "Issues and challenges facing rechargeable lithium batteries," (in English), *Nature,* vol. 414, no. 6861, pp. 359-367, Nov 15 2001.

[6] Q. Y. Huang, D. R. Wang, and Z. J. Zheng, "Textile-Based Electrochemical Energy Storage Devices," (in English), *Advanced Energy Materials,* vol. 6, no. 22, Nov 23 2016.

[7] O. Adesina, I. A. Anzai, J. L. Avalos, and B. Barstow, "Embracing Biological Solutions to the Sustainable Energy Challenge," (in English), *Chem,* vol. 2, no. 1, pp. 20-51, Jan 12 2017.

[8] M. A. Hannan, M. M. Hoque, A. Mohamed, and A. Ayob, "Review of energy storage systems for electric vehicle applications: Issues and challenges," (in

English), *Renewable & Sustainable Energy Reviews*, vol. 69, pp. 771-789, Mar 2017.

[9] K. Kleiner and H. Ehrenberg, "Challenges Considering the Degradation of Cell Components in Commercial Lithium-Ion Cells: A Review and Evaluation of Present Systems," (in English), *Topics in Current Chemistry*, vol. 375, no. 3, Jun 2017.

[10] C. S. Lai and M. D. McCulloch, "Levelized cost of electricity for solar photovoltaic and electrical energy storage," (in English), *Applied Energy*, vol. 190, pp. 191-203, Mar 15 2017.

[11] C. Li, Z. B. Wang, Q. Wang, and D. M. Gu, "Recent advances in cathode materials for Li-S battery: structure and performance," (in English), *Rare Metals*, vol. 36, no. 5, pp. 365-380, May 2017.

[12] Y. Li, J. Yang, and J. Song, "Design structure model and renewable energy technology for rechargeable battery towards greener and more sustainable electric vehicle," (in English), *Renewable & Sustainable Energy Reviews*, vol. 74, pp. 19-25, Jul 2017.

[13] M. Mussard, "Solar energy under cold climatic conditions: A review," (in English), *Renewable & Sustainable Energy Reviews*, vol. 74, pp. 733-745, Jul 2017.

[14] S. Rashidi, J. A. Esfahani, and A. Rashidi, "A review on the applications of porous materials in solar energy systems," (in English), *Renewable & Sustainable Energy Reviews*, vol. 73, pp. 1198-1210, Jun 2017.

[15] H. Wang, Y. Yang, and L. Guo, "Nature-Inspired Electrochemical Energy-Storage Materials and Devices," (in English), *Advanced Energy Materials,* vol. 7, no. 5, Mar 8 2017.

[16] M. Winter and R. J. Brodd, "What are batteries, fuel cells, and supercapacitors? (vol 104, pg 4245, 2003)," (in English), *Chemical Reviews,* vol. 105, no. 3, pp. 1021-1021, Mar 2005.

[17] J. F. Chen *et al.*, "The Origin of Improved Electrical Double-Layer Capacitance by Inclusion of Topological Defects and Dopants in Graphene for Supercapacitors," (in English), *Angewandte Chemie-International Edition,* vol. 55, no. 44, pp. 13822-13827, Oct 24 2016.

[18] K. A. Francis, C. W. Liew, S. Ramesh, K. Ramesh, and S. Ramesh, "Ionic liquid enhanced magnesium-based polymer electrolytes for electrical double-layer capacitors," (in English), *Ionics,* vol. 22, no. 6, pp. 919-925, Jun 2016.

[19] A. Orphanou, T. Yamada, and C. Y. Yang, "Optimization of carbon nanotube ultracapacitor for cell design," (in English), *Journal of Applied Physics,* vol. 119, no. 21, Jun 7 2016.

[20] K. S. Sulaiman, A. Mat, and A. K. Arof, "Activated carbon from coconut leaves for electrical double-layer capacitor," (in English), *Ionics,* vol. 22, no. 6, pp. 911-918, Jun 2016.

[21] Y. F. Wang and S. L. Zuo, "Electrochemical Properties of Phosphorus-Containing Activated Carbon Electrodes on Electrical Double-Layer Capacitors," (in Chinese), *Acta Physico-Chimica Sinica,* vol. 32, no. 2, pp. 481-492, Feb 2016.

[22] K. L. Wang, M. Xu, Y. Gu, Z. R. Gu, J. Liu, and Q. H. Fan, "Low-temperature plasma exfoliated n-doped graphene for symmetrical electrode supercapacitors," (in English), *Nano Energy*, vol. 31, pp. 486-494, Jan 2017.

[23] J. P. Schmidt, H. Y. Tran, J. Richter, E. Ivers-Tiffee, and M. Wohlfahrt-Mehrens, "Analysis and prediction of the open circuit potential of lithium-ion cells," (in English), *Journal of Power Sources*, vol. 239, pp. 696-704, Oct 1 2013.

[24] F. Schipper and D. Aurbach, "A Brief Review: Past, Present and Future of Lithium Ion Batteries," (in English), *Russian Journal of Electrochemistry*, vol. 52, no. 12, pp. 1095-1121, Dec 2016.

[25] D. Grazioli, M. Magri, and A. Salvadori, "Computational modeling of Li-ion batteries," (in English), *Computational Mechanics*, vol. 58, no. 6, pp. 889-909, Dec 2016.

[26] M. S. Whittingham, "Lithium batteries and cathode materials," (in English), *Chemical Reviews*, vol. 104, no. 10, pp. 4271-4301, Oct 2004.

[27] S. S. Fan, H. Zhong, H. T. Yu, M. Lou, Y. Xie, and Y. R. Zhu, "Hollow and hierarchical Na2Li2Ti6O14 microspheres with high electrochemical performance as anode material for lithium-ion battery," (in English), *Science China-Materials*, vol. 60, no. 5, pp. 427-437, May 2017.

[28] X. Y. Feng, X. Li, M. X. Tang, A. Gan, and Y. Y. Hu, "Enhanced rate performance of Li4Ti5O12 anodes with bridged grain boundaries," (in English), *Journal of Power Sources*, vol. 354, pp. 172-178, Jun 30 2017.

[29] J. Kim, E. Yamasue, H. Okumura, C. Michioka, and K. N. Ishihara, "Intercalation of hexagonal boron nitride and graphite with lithium by sequential process of ball milling and heat treatment," (in English), *Journal of Alloys and Compounds,* vol. 707, pp. 172-177, Jun 15 2017.

[30] S. X. Wu, K. S. Hui, K. N. Hui, J. M. Yun, and K. H. Kim, "A novel approach to fabricate carbon sphere intercalated holey graphene electrode for high energy density electrochemical capacitors," (in English), *Chemical Engineering Journal,* vol. 317, pp. 461-470, Jun 1 2017.

[31] J. G. Xu, R. D. Deshpande, J. Pan, Y. T. Cheng, and V. S. Battaglia, "Electrode Side Reactions, Capacity Loss and Mechanical Degradation in Lithium-Ion Batteries," (in English), *Journal of the Electrochemical Society,* vol. 162, no. 10, pp. A2026-A2035, 2015.

[32] X. Xu, Z. G. Li, and N. Chen, "A Hierarchical Model for Lithium-Ion Battery Degradation Prediction," (in English), *Ieee Transactions on Reliability,* vol. 65, no. 1, pp. 310-325, Mar 2016.

[33] T. Yoshida *et al.*, "Degradation mechanism and life prediction of lithium-ion batteries," (in English), *Journal of the Electrochemical Society,* vol. 153, no. 3, pp. A576-A582, 2006.

[34] S. Shiotani *et al.*, "Degradation analysis of 18650-type lithium-ion cells by operando neutron diffraction," (in English), *Journal of Power Sources,* vol. 325, pp. 404-409, Sep 1 2016.

[35] X. Su *et al.*, "A new strategy to mitigate the initial capacity loss of lithium ion batteries," (in English), *Journal of Power Sources*, vol. 324, pp. 150-157, Aug 30 2016.

[36] P. Keil and A. Jossen, "Calendar Aging of NCA Lithium-Ion Batteries Investigated by Differential Voltage Analysis and Coulomb Tracking," (in English), *Journal of the Electrochemical Society*, vol. 164, no. 1, pp. A6066-A6074, 2017.

[37] K. Liu *et al.*, "Lithium Metal Anodes with an Adaptive "Solid-Liquid" Interfacial Protective Layer," (in English), *Journal of the American Chemical Society*, vol. 139, no. 13, pp. 4815-4820, Apr 5 2017.

[38] J. Yi, B. Koo, C. B. Shin, T. Han, and S. Park, "Modeling the effect of aging on the electrical and thermal behaviors of a lithium-ion battery during constant current charge and discharge cycling," (in English), *Computers & Chemical Engineering*, vol. 99, pp. 31-39, Apr 6 2017.

[39] J. Cannarella and C. B. Arnold, "The Effects of Defects on Localized Plating in Lithium-Ion Batteries," (in English), *Journal of the Electrochemical Society*, vol. 162, no. 7, pp. A1365-A1373, 2015.

[40] B. Ahmed, C. Xia, and H. N. Alshareef, "Electrode surface engineering by atomic layer deposition: A promising pathway toward better energy storage," (in English), *Nano Today*, vol. 11, no. 2, pp. 250-271, Apr 2016.

[41] X. B. Cheng, R. Zhang, C. Z. Zhao, F. Wei, J. G. Zhang, and Q. Zhang, "A Review of Solid Electrolyte Interphases on Lithium Metal Anode," (in English), *Advanced Science*, vol. 3, no. 3, Mar 2016.

[42] N. A. A. Aziz, M. De Cunha, T. K. Abdullah, and A. A. Mohamad, "Degradation of LiCoO2 in aqueous lithium-air batteries," (in English), *International Journal of Energy Research*, vol. 41, no. 2, pp. 289-296, Feb 2017.

[43] C. R. Birkl, M. R. Roberts, E. McTurk, P. G. Bruce, and D. A. Howey, "Degradation diagnostics for lithium ion cells," (in English), *Journal of Power Sources*, vol. 341, pp. 373-386, Feb 15 2017.

[44] H. Ge *et al.*, "Investigating Lithium Plating in Lithium-Ion Batteries at Low Temperatures Using Electrochemical Model with NMR Assisted Parameterization," (in English), *Journal of the Electrochemical Society*, vol. 164, no. 6, pp. A1050-A1060, 2017.

[45] M. Haruta *et al.*, "Temperature effects on SEI formation and cyclability of Si nanoflake powder anode in the presence of SEI-forming additives," (in English), *Electrochimica Acta*, vol. 224, pp. 186-193, Jan 10 2017.

[46] N. Paul *et al.*, "Aging behavior of lithium iron phosphate based 18650-type cells studied by in situ neutron diffraction," (in English), *Journal of Power Sources*, vol. 345, pp. 85-96, Mar 31 2017.

[47] G. Y. Wang *et al.*, "How to improve the stability and rate performance of lithium-ion batteries with transition metal oxide anodes," (in English), *Journal of Materials Research*, vol. 32, no. 1, pp. 16-36, Jan 2017.

[48] J. G. Lee *et al.*, "Mechanical Damage of Surface Films and Failure of Nano-Sized Silicon Electrodes in Lithium Ion Batteries," (in English), *Journal of the Electrochemical Society*, vol. 164, no. 1, pp. A6103-A6109, 2017.

[49] S. B. Lee and S. I. Pyun, "The effect of electrolyte temperature on the passivity of solid electrolyte interphase formed on a graphite electrode," (in English), *Carbon*, vol. 40, no. 13, pp. 2333-2339, 2002.

[50] A. Augustsson *et al.*, "Solid electrolyte interphase on graphite Li-ion battery anodes studied by soft X-ray spectroscopy," (in English), *Physical Chemistry Chemical Physics*, vol. 6, no. 16, pp. 4185-4189, 2004.

[51] H. Buqa *et al.*, "Negative Electrodes in Rechargeable Lithium Ion Batteries - Influence of Graphite Surface Modification on the Formation of the Solid Electrolyte Interphase," (in English), *Ionics*, vol. 6, no. 3-4, pp. 172-179, May 2000.

[52] C. F. Chen, P. Barai, and P. P. Mukherjee, "An overview of degradation phenomena modeling in lithium-ion battery electrodes," (in English), *Current Opinion in Chemical Engineering*, vol. 13, pp. 82-90, Aug 2016.

[53] Y. L. He, H. J. Hu, K. F. Zhang, S. Li, and J. H. Chen, "Mechanical insights into the stability of heterogeneous solid electrolyte interphase on an electrode particle," (in English), *Journal of Materials Science*, vol. 52, no. 5, pp. 2836-2848, Mar 2017.

[54] L. M. Kasmaee, A. Aryanfar, Z. Chikneyan, M. R. Hoffmann, and A. J. Colussi, "Lithium batteries: Improving solid-electrolyte interphases via underpotential solvent electropolymerization," (in English), *Chemical Physics Letters*, vol. 661, pp. 65-69, Sep 16 2016.

[55] R. Kumar *et al.*, "In Situ and Operando Investigations of Failure Mechanisms of the Solid Electrolyte Interphase on Silicon Electrodes," (in English), *Acs Energy Letters*, vol. 1, no. 4, pp. 689-697, Oct 2016.

[56] Y. Liu, B. F. Wang, J. Y. Xie, J. Yang, and J. Chen, "Electrochemical characteristic of SEI in secondary lithium batteries," (in Chinese), *Journal of Inorganic Materials*, vol. 18, no. 2, pp. 307-312, Mar 2003.

[57] A. Moradabadi, M. Bakhtiari, and P. Kaghazchi, "Effect of Anode Composition on Solid Electrolyte Interphase Formation," (in English), *Electrochimica Acta*, vol. 213, pp. 8-13, Sep 20 2016.

[58] M. B. Pinson and M. Z. Bazant, "Theory of SEI Formation in Rechargeable Batteries: Capacity Fade, Accelerated Aging and Lifetime Prediction," (in English), *Journal of the Electrochemical Society*, vol. 160, no. 2, pp. A243-A250, 2013.

[59] A. Mukhopadhyay and B. W. Sheldon, "Deformation and stress in electrode materials for Li-ion batteries," (in English), *Progress in Materials Science*, vol. 63, pp. 58-116, Jun 2014.

[60] K. D. Kepler, J. T. Vaughey, and M. M. Thackeray, "Copper-tin anodes for rechargeable lithium batteries: an example of the matrix effect in an intermetallic system," (in English), *Journal of Power Sources*, vol. 81, pp. 383-387, Sep 1999.

[61] K. D. Kepler, J. T. Vaughey, and M. M. Thackeray, "Li(x)Cu(6)Sn(5) ($0 < x < 13$): An intermetallic insertion electrode for rechargeable lithium batteries," (in

English), *Electrochemical and Solid State Letters,* vol. 2, no. 7, pp. 307-309, Jul 1999.

[62] J. Wolfenstine, S. Campos, D. Foster, J. Read, and W. K. Behl, "Nano-scale Cu6Sn5 anodes," (in English), *Journal of Power Sources,* vol. 109, no. 1, pp. 230-233, Jun 15 2002.

[63] H. C. Shin and M. L. Liu, "Three-dimensional porous copper-tin alloy electrodes for rechargeable lithium batteries," (in English), *Advanced Functional Materials,* vol. 15, no. 4, pp. 582-586, Apr 2005.

[64] L. Trahey, J. T. Vaughey, H. H. Kung, and M. M. Thackeray, "High-Capacity, Microporous Cu6Sn5-Sn Anodes for Li-Ion Batteries," (in English), *Journal of the Electrochemical Society,* vol. 156, no. 5, pp. A385-A389, 2009.

[65] W. J. Zhang, "A review of the electrochemical performance of alloy anodes for lithium-ion batteries," (in English), *Journal of Power Sources,* vol. 196, no. 1, pp. 13-24, Jan 1 2011.

[66] F. Wang, J. Yi, Y. G. Wang, and Y. Y. Xia, "A reduced graphene oxide/Cu6Sn5 nanocomposite with enhanced cycling stability for lithium storage," (in English), *Nanotechnology,* vol. 24, no. 42, Oct 25 2013.

[67] R. Z. Hu *et al.*, "Cu6Sn5@SnO2-C nanocomposite with stable core/shell structure as a high reversible anode for Li-ion batteries," (in English), *Nano Energy,* vol. 18, pp. 232-244, Nov 2015.

[68] P. T. Dirlam, R. S. Glass, K. Char, and J. Pyun, "The Use of Polymers in Li-S Batteries: A Review," (in English), *Journal of Polymer Science Part a-Polymer Chemistry*, vol. 55, no. 10, pp. 1635-1668, May 15 2017.

[69] L. M. Jin, G. R. Li, B. H. Liu, Z. P. Li, J. S. Zheng, and J. P. Zheng, "A novel strategy for high-stability lithium sulfur batteries by in situ formation of polysulfide adsorptive-blocking layer," (in English), *Journal of Power Sources*, vol. 355, pp. 147-153, Jul 1 2017.

[70] L. C. Zeng, W. H. Li, Y. Jiang, and Y. Yu, "Recent progress in Li-S and Li-Se batteries," (in English), *Rare Metals*, vol. 36, no. 5, pp. 339-364, May 2017.

[71] B. Bitzer and A. Gruhle, "A new method for detecting lithium plating by measuring the cell thickness," (in English), *Journal of Power Sources*, vol. 262, pp. 297-302, Sep 15 2014.

[72] J. C. Burns, D. A. Stevens, and J. R. Dahn, "In-Situ Detection of Lithium Plating Using High Precision Coulometry," (in English), *Journal of the Electrochemical Society*, vol. 162, no. 6, pp. A959-A964, 2015.

[73] N. Ghanbari, T. Waldmann, M. Kasper, P. Axmann, and M. Wohlfahrt-Mehrens, "Detection of Li Deposition by Glow Discharge Optical Emission Spectroscopy in Post-Mortem Analysis," (in English), *Ecs Electrochemistry Letters*, vol. 4, no. 9, pp. A100-A102, 2015.

[74] M. Petzl and M. A. Danzer, "Nondestructive detection, characterization, and quantification of lithium plating in commercial lithium-ion batteries," (in English), *Journal of Power Sources*, vol. 254, pp. 80-87, May 15 2014.

[75] M. Petzl, M. Kasper, and M. A. Danzer, "Lithium plating in a commercial lithium-ion battery A low-temperature aging study," (in English), *Journal of Power Sources,* vol. 275, pp. 799-807, Feb 1 2015.

[76] C. Uhlmann, J. Illig, M. Ender, R. Schuster, and E. Ivers-Tiffee, "In situ detection of lithium metal plating on graphite in experimental cells," (in English), *Journal of Power Sources,* vol. 279, pp. 428-438, Apr 1 2015.

[77] V. Zinth *et al.*, "Lithium plating in lithium-ion batteries at sub-ambient temperatures investigated by in situ neutron diffraction," (in English), *Journal of Power Sources,* vol. 271, pp. 152-159, Dec 20 2014.

[78] L. Gireaud, S. Grugeon, S. Laruelle, B. Yrieix, and J. M. Tarascon, "Lithium metal stripping/plating mechanisms studies: A metallurgical approach," (in English), *Electrochemistry Communications,* vol. 8, no. 10, pp. 1639-1649, Oct 2006.

[79] W. D. Zhou, S. F. Wang, Y. T. Li, S. Xin, A. Manthiram, and J. B. Goodenough, "Plating a Dendrite-Free Lithium Anode with a Polymer/Ceramic/Polymer Sandwich Electrolyte," (in English), *Journal of the American Chemical Society,* vol. 138, no. 30, pp. 9385-9388, Aug 3 2016.

[80] Y. J. Li, J. Y. Jiao, J. P. Bi, X. F. Wang, Z. X. Wang, and L. Q. Chen, "Controlled deposition of Li metal," (in English), *Nano Energy,* vol. 32, pp. 241-246, Feb 2017.

[81] A. Pei, G. Y. Zheng, F. F. Shi, Y. Z. Li, and Y. Cui, "Nanoscale Nucleation and Growth of Electrodeposited Lithium Metal," (in English), *Nano Letters,* vol. 17, no. 2, pp. 1132-1139, Feb 2017.

[82] B. Y. Xu *et al.*, "Li3PO4-added garnet-type Li6.5La3Zr1.5Ta0.5O12 for Li-dendrite suppression," (in English), *Journal of Power Sources,* vol. 354, pp. 68-73, Jun 30 2017.

[83] R. Zhang, N. W. Li, X. B. Cheng, Y. X. Yin, Q. Zhang, and Y. G. Guo, "Advanced Micro/Nanostructures for Lithium Metal Anodes," (in English), *Advanced Science,* vol. 4, no. 3, Mar 2017.

[84] T. Waldmann *et al.*, "Interplay of Operational Parameters on Lithium Deposition in Lithium-Ion Cells: Systematic Measurements with Reconstructed 3-Electrode Pouch Full Cells," (in English), *Journal of the Electrochemical Society,* vol. 163, no. 7, pp. A1232-A1238, 2016.

[85] J. W. Tan, A. M. Tartakovsky, K. Ferris, and E. M. Ryan, "Investigating the Effects of Anisotropic Mass Transport on Dendrite Growth in High Energy Density Lithium Batteries," (in English), *Journal of the Electrochemical Society,* vol. 163, no. 2, pp. A318-A327, 2016.

[86] F. La Mantia, C. D. Wessells, H. D. Deshazer, and Y. Cui, "Reliable reference electrodes for lithium-ion batteries," (in English), *Electrochemistry Communications,* vol. 31, pp. 141-144, Jun 2013.

[87] J. R. Belt, D. M. Bernardi, and V. Utgikar, "Development and Use of a Lithium-Metal Reference Electrode in Aging Studies of Lithium-Ion Batteries," (in English), *Journal of the Electrochemical Society,* vol. 161, no. 6, pp. A1116-A1126, 2014.

[88] S. Solchenbach, D. Pritzl, E. J. Y. Kong, J. Landesfeind, and H. A. Gasteiger, "A Gold Micro-Reference Electrode for Impedance and Potential Measurements in Lithium Ion Batteries," *Journal of The Electrochemical Society,* vol. 163, no. 10, pp. A2265-A2272, 2016.

[89] A. N. Jansen, D. W. Dees, D. P. Abraham, K. Amine, and G. L. Henriksen, "Low-temperature study of lithium-ion cells using a LiySn micro-reference electrode," (in English), *Journal of Power Sources,* vol. 174, no. 2, pp. 373-379, Dec 6 2007.

[90] D. P. Abraham, S. D. Poppen, A. N. Jansen, J. Liu, and D. W. Dees, "Application of a lithium-tin reference electrode to determine electrode contributions to impedance rise in high-power lithium-ion cells," (in English), *Electrochimica Acta,* vol. 49, no. 26, pp. 4763-4775, Oct 15 2004.

[91] S. Wennig *et al.,* "The influence of different pre-treatments of current collectors and variation of the binders on the performance of Li4Ti5O12 anodes for lithium ion batteries," (in English), *Journal of Applied Electrochemistry,* vol. 45, no. 10, pp. 1043-1055, Oct 2015.

[92] K. Nakahara, R. Nakajima, T. Matsushima, and H. Majima, "Preparation of particulate Li4Ti5O12 having excellent characteristics as an electrode active material for power storage cells," (in English), *Journal of Power Sources,* vol. 117, no. 1-2, pp. 131-136, May 15 2003.

[93] Y. Shi, L. Wen, F. Li, and H. M. Cheng, "Nanosized Li4Ti5O12/graphene hybrid materials with low polarization for high rate lithium ion batteries," (in English), *Journal of Power Sources,* vol. 196, no. 20, pp. 8610-8617, Oct 15 2011.

[94] E. Ferg, R. J. Gummow, A. Dekock, and M. M. Thackeray, "Spinel Anodes for Lithium-Ion Batteries," (in English), *Journal of the Electrochemical Society,* vol. 141, no. 11, pp. L147-L150, Nov 1994.

[95] J. R. Li, Z. L. Tang, and Z. T. Zhang, "Controllable formation and electrochemical properties of one-dimensional nanostructured spinel Li4Ti5O12," (in English), *Electrochemistry Communications,* vol. 7, no. 9, pp. 894-899, Sep 2005.

[96] D. W. Dees, A. N. Jansen, and D. P. Abraham, "Theoretical examination of reference electrodes for lithium-ion cells," (in English), *Journal of Power Sources,* vol. 174, no. 2, pp. 1001-1006, Dec 6 2007.

[97] B. R. Long *et al.*, "Enabling High-Energy, High-Voltage Lithium-Ion Cells: Standardization of Coin-Cell Assembly, Electrochemical Testing, and Evaluation of Full Cells," *Journal of The Electrochemical Society,* vol. 163, no. 14, pp. A2999-A3009, 2016.

[98] M. S. Wu, P. C. J. Chiang, and J. C. Lin, "Electrochemical investigations on advanced lithium-ion batteries by three-electrode measurements," (in English), *Journal of the Electrochemical Society,* vol. 152, no. 1, pp. A47-A52, 2005.

[99] M. Ender, A. Weber, and E. Ivers-Tiffee, "Analysis of Three-Electrode Setups for AC-Impedance Measurements on Lithium-Ion Cells by FEM simulations," (in English), *Journal of the Electrochemical Society,* vol. 159, no. 2, pp. A128-A136, 2012.

[100] M. Ender, J. Illig, and E. Ivers-Tiffée, "Three-Electrode Setups for Lithium-Ion Batteries I. Fem-Simulation of Different Reference Electrode Designs and Their

Implications for Half-Cell Impedance Spectra," *Journal of The Electrochemical Society*, vol. 164, no. 2, pp. A71-A79, 2017.

[101] E. McTurk, C. R. Birkl, M. R. Roberts, D. A. Howey, and P. G. Bruce, "Minimally Invasive Insertion of Reference Electrodes into Commercial Lithium-Ion Pouch Cells," (in English), *Ecs Electrochemistry Letters*, vol. 4, no. 12, pp. A145-A147, 2015.

[102] T. Waldmann, M. Kasper, and M. Wohlfahrt-Mehrens, "Optimization of Charging Strategy by Prevention of Lithium Deposition on Anodes in high-energy Lithium-ion Batteries - Electrochemical Experiments," (in English), *Electrochimica Acta*, vol. 178, pp. 525-532, Oct 1 2015.

[103] K. Zaghib, M. Simoneau, M. Armand, and M. Gauthier, "Electrochemical study of Li4Ti5O12 as negative electrode for Li-ion polymer rechargeable batteries," (in English), *Journal of Power Sources*, vol. 81, pp. 300-305, Sep 1999.